A pre-processing methodology to enhance novel information for rotating machine diagnostics

Stephan Schmidt[a,*], P. Stephan Heyns[a], Konstantinos C. Gryllias[b,c]

[a] *Centre for Asset Integrity Management, Department of Mechanical and Aeronautical Engineering, University of Pretoria, Pretoria, South Africa*
[b] *Department of Mechanical Engineering, PMA Division, KU Leuven, Celestijnenlaan 300, 3001 Heverlee, Belgium*
[c] *Dynamics of Mechanical and Mechatronic Systems, Flanders Make, Belgium*

Abstract

Many sophisticated signal analysis techniques are developed to efficiently detect, localise and trend damage in rotating machine components such as bearings and gears for example. However, these techniques are generally applied without effectively incorporating historical information when performing condition monitoring. It is possible to enhance the performance of the analysis techniques by incorporating historical data from a machine in a reference condition. In this paper, a methodology is proposed to extract a novel signal i.e. a signal that contains information that is not present in the historical reference data, from a vibration signal. This is performed by utilising the available historical data. Sophisticated signal analysis techniques can subsequently be used on the novel vibration signal to diagnose the machine. The benefits of the methodology are illustrated on data, generated from phenomenological gearbox model data and experimental gearbox data, by utilising advanced techniques based on cyclostationary analysis. The results indicate that the novel vibration signal is more sensitive to damage, which highlights its potential as a pre-processing technique for rotating machine applications where historical data are available.

Keywords:
Gearbox diagnostics, Novel information enhancement, Historical reference data,
Cyclostationary analysis

1. Introduction

Condition-based maintenance uses processed condition monitoring data as basis for maintenance decisions and is important to ensure that expensive rotating machines operate cost-

*Corresponding author.
Email address: stephanschmidt@zoho.com (Stephan Schmidt)

effectively and reliably [1]. In vibration-based condition monitoring, signal processing and analysis techniques form an integral part of diagnosing the machine; they are used to highlight diagnostic information and to attenuate extraneous components. Many traditional signal analysis techniques such as frequency domain analysis are inadequate for incipient fault detection and therefore more sophisticated techniques are researched for rotating machine diagnostics [2–5].

One of the most powerful approaches to rotating machine diagnostics is based on cyclostationary analysis. Cyclostationary analysis techniques are well suited for diagnosing rotating machines, because rotating machine vibration signals are generated by periodic mechanisms which result in the signals having periodic statistical properties [6]. The vibration signals are time or angle cyclostationary under stationary operating conditions [6] and the signals are cyclo-non-stationary under non-stationary speed conditions [7]. The associated analysis techniques are given in Refs. [3, 7–11]

Envelope analysis is one of the most popular cyclostationary techniques for bearing diagnostics [5, 12, 13]. The Squared Envelope Spectrum (SES) is sensitive to the presence of second-order cyclostationary vibration components and is therefore ideal for detecting bearing damage. However, it is necessary to remove interfering signal components from the vibration signal prior to envelope analysis. This is achieved by either bandpass filtering the signal to retain the information pertaining to the excited resonance frequencies or performing envelope analysis on the residual signal [12, 14].

The optimal properties of the bandpass filter for envelope analysis i.e. the required centre frequency and the bandwidth are unknown when performed without historical fault data and need to be estimated from the data. Bearing damage results in the impulsive content of specific frequency bands to increase, which makes the spectral kurtosis an ideal tool for identifying the aforementioned frequency bands. The spectral kurtosis provides an estimation of the impulsiveness of different frequency bands and is calculated with time-frequency estimators [15]. However, the estimated spectral kurtosis is sensitive to the frequency resolution of the time-frequency decomposition. This shortcoming is circumvented with the kurtogram, where time-frequency decompositions with different frequency resolutions are performed whereafter the centre frequency and frequency resolution that maximises the spectral kurtosis are selected [15–17]. The spectral kurtosis and kurtogram are powerful techniques for detecting faults such as gear [16, 18, 19] and bearing faults [5, 16].

However, the spectral kurtosis is sensitive to spurious impulsive noise which can result in the wrong frequency band to be detected and subsequently the wrong bandpass filter to be used for

envelope analysis [20]. Also, the spectral kurtosis decreases as the repetition rate of the impulses increases [20]. The aforementioned shortcomings have resulted in many improvements to the spectral kurtosis to be proposed; for example the protrugram [21], the improved kurtogram [22], the enhanced kurtogram [23], an optimised spectral kurtosis [24], the sparsogram [25], informative frequency band selectors [26], the envelope harmonic-to-noise ratio decomposition [27], the autogram [28] and the infogram [20, 29, 30] can be used as alternatives to the spectral kurtosis or kurtogram.

These fault diagnosis methods are usually implemented without using historical data. Even though historical fault data are expensive and often impractical to acquire, historical data of a healthy machine or a machine in a reference condition can easily be acquired in many circumstances. It could be advantageous to use fault diagnosis methods that incorporate information from historical data or a reference condition into the diagnosis procedure. Randall [31] used the difference in the spectrum of a gearbox with a rolling element fault and an identical healthy gearbox to determine a frequency band for envelope analysis. Fernández-Francos et al. [32] used a support vector machine, optimised on healthy data, to select the frequency band for envelope analysis. Klein et al. [33] used image processing methods to develop a fault diagnosis methodology that enhances novel information in a RPM-order representation.

In condition monitoring, the characteristics of the data (e.g. spectral content) are investigated for changes from a reference condition. However, it could be beneficial to have a signal that only contains changes from a reference condition i.e. novel information and then to subsequently analyse this signal for potential diagnostic information using conventional fault diagnosis techniques. Hence, in this paper, a pre-processing methodology is proposed that utilises the available historical reference data to enhance novel information in the vibration signal. A novel information filter is designed which passes frequency bands with significant changes in its statistical characteristics with respect to the reference condition and attenuates frequency bands that do not contain any novel information. The resulting signal is rich with novel information and is referred to as the novel signal. The novel signal is then subsequently analysed using signal analysis techniques for the presence of damage. In this work, cyclostationary analysis techniques are used to analyse the original and novel signals.

In summary, the benefits of this methodology are:

- Historical reference data can be incorporated as a pre-processing technique, whereafter conventional fault diagnosis techniques can be applied.

- The filter is designed by considering the statistical properties of the frequency bands. This makes the approach sensitive to small changes in the statistical properties of specific frequency bands.

- It is not necessary to select a single frequency band to perform envelope analysis as done with the kurtogram and related methods. Multiple frequency bands can automatically be selected which for example allows envelope analysis to be performed over the full bandwidth of the novel vibration signal.

In the next section, the methodology is presented, whereafter the methodology is investigated on phenomenological gearbox data in Section 3 and experimental gearbox data in Section 4. Finally, conclusions are drawn and recommendations are made in Section 5. Appendix A contains supporting information related to the phenomenological gearbox data in Section 3 and Appendix B contains additional information related to the proposed quality metrics used in Section 4.

2. Methodology

We desire to extract a novel signal $\boldsymbol{x}_{novel} \in \mathbb{R}^{N_x \times 1}$ from a measured vibration signal $\boldsymbol{x} = [x[0], x[1], \dots x[N_x - 1]]^T$ with N_x samples i.e. $\boldsymbol{x} \in \mathbb{R}^{N_x \times 1}$ by using a dataset from the machine in a reference condition. The reference dataset contains N_{train} measurements and is denoted by $\left\{\boldsymbol{x}_{train}^{(i)}\right\}$, $i = 0, \dots N_{train} - 1$.

A methodology is presented in Figure 1 to extract the novel signal from a newly acquired vibration signal. This novel signal represents the deviation between the newly acquired vibration signal and the vibration signal generated by the healthy gearbox. Therefore, if the gearbox is damaged, the novel signal would be rich with fault-related information. The methodology consists

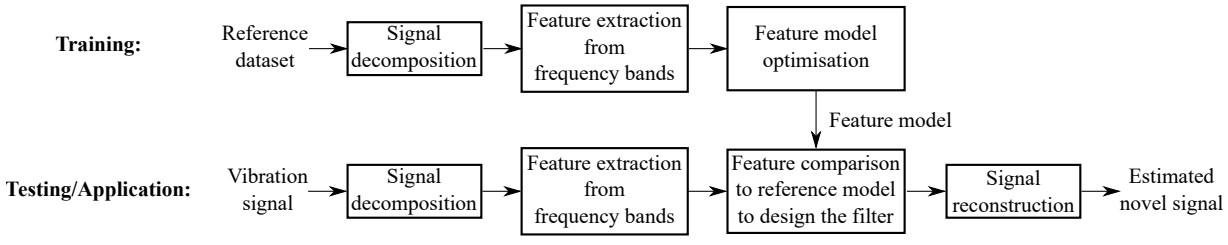

Figure 1: An overview of the methodology

of two main phases, namely a training phase and a testing phase. The training phase is used to obtain the model parameters through a model optimisation process on the reference dataset.

The testing phase uses the model parameters to design a filter that is used to extract a novel signal that corresponds to the input vibration signal.

A detailed overview of each step in the methodology is given in subsequent sections.

2.1. Signal decomposition and feature extraction

We make the assumption that the machine component damage manifests in specific frequency bands and results in changes in the statistical properties of the associated feature bands e.g. the damage results in the impulsiveness to increase. Hence, features are extracted from narrowband signals to detect changes in the statistical properties of the frequency bands.

The first step of the feature extraction procedure is to decompose the signal into a time-frequency representation. The Short-Time Fourier Transform (STFT) of the signal $\boldsymbol{x} \in \mathbb{R}^{N_x \times 1}$,

$$S_x[n, m; \Delta f_l] = \sum_{k=0}^{N_w - 1} x[n \cdot (N_w - N_o) + k] \cdot \upsilon[k] \cdot e^{-j2\pi k m \frac{\Delta f_l}{f_s}} \tag{1}$$

is used for this task. The STFT is calculated for a pre-determined frequency resolution Δf_l and a corresponding time resolution Δt_l, with the time step and frequency that correspond to $S_x[n, m; \Delta f_l]$ given by $t = n\Delta t_l$ and $f = m\Delta f_l$, respectively. The windowing function $\boldsymbol{\upsilon} \in \mathbb{R}^{N_w \times 1}$ can for example be a Hann function, where N_w is the length of the discrete window function and N_o denotes the number of samples overlapping between consecutive windows. The sampling frequency of the signal $\boldsymbol{x}$ is denoted by f_s.

The optimal window length for the STFT for machine diagnostics depends on the rotational speed of the component [19, 21] and therefore under varying speed conditions the optimal window length becomes difficult to be estimated. Therefore, in this methodology N_l time-frequency decompositions are investigated to alleviate the influence of varying speed conditions. The novel information, detected in the different time-frequency distributions, is combined to obtain a single novel signal with the method discussed in Section 2.4. In the investigations performed in this paper, a Hann window is used for all decomposition levels, with the following window lengths $\{N_w\} = \{8, 16, 32, 64, 128, 256, 512, 1024, 2048\}$ and a 75% overlap between consecutive windows being used.

A feature extraction function Ψ_{feat} is used to extract a diagnostic feature $\mathcal{U}(f, \Delta f_l)$ from the temporal signal associated with each centre frequency $f = m \cdot \Delta f_l$ of the STFT with a frequency resolution of Δf_l

$$\mathcal{U}(m \cdot \Delta f_l, \Delta f_l) = \Psi_{feat}(S_x[n, m; \Delta f_l]). \tag{2}$$

The feature extraction function Ψ_{feat} can be used to extract the kurtosis of the bandlimited signals, whereafter the kurtogram [15]

$$\mathcal{U}\left(m \cdot \Delta f_l, \Delta f_l\right) = \frac{\left\langle \left|S_x[n, m; \Delta f_l]\right|^4 \right\rangle_n}{\left\langle \left|S_x[n, m; \Delta f_l]\right|^2 \right\rangle_n^2} - 2, \tag{3}$$

is obtained. The squared envelope negentropy can also be extracted which results in the squared envelope infogram [20]

$$\mathcal{U}\left(m \cdot \Delta f_l, \Delta f_l\right) = \left\langle \frac{\left|S_x[n, m; \Delta f_l]\right|^2}{\left\langle \left|S_x[n, m; \Delta f_l]\right|^2 \right\rangle_n} \log\left(\frac{\left|S_x[n, m; \Delta f_l]\right|^2}{\left\langle \left|S_x[n, m; \Delta f_l]\right|^2 \right\rangle_n} \right) \right\rangle_n \tag{4}$$

or the kurtosis and the squared envelope negentropy can for example simultaneously be used as features. In Equations (3) and (4), $\langle \cdot \rangle_n$ denotes the time averaging operator over N_t time steps e.g.

$$\langle |S_x[n, m; \Delta f_l]| \rangle_n = \frac{1}{N_t} \sum_{n=0}^{N_t - 1} |S_x[n, m; \Delta f_l]|. \tag{5}$$

The N_{feat} features extracted from the different frequency bands of the N_l STFT decompositions are written as a vector $\boldsymbol{u} \in \mathbb{R}^{N_{feat}}$ to simplify the notation and computations used in the subsequent sections. The features that correspond to the reference dataset are denoted by $\{\boldsymbol{u}_{train}^{(i)}\}, i = 0, \ldots, N_{train} - 1$ and is the training dataset that is modelled in the next section.

2.2. Feature modelling

In this step of the process, it is necessary to determine whether the features of specific frequency bands conform to the expected behaviour governed by the probability density function of the reference features or whether there is novelty in that region.

The features $\boldsymbol{u}$ are parametrised by the Gaussian Probability Density Function (PDF)

$$p(\boldsymbol{u}; \boldsymbol{\mu}_u, \boldsymbol{\Sigma}_u) = \frac{1}{(2\pi)^{N_{feat}/2}} \frac{1}{|\boldsymbol{\Sigma}_u|^{1/2}} \exp\left(-\frac{1}{2} \left(\boldsymbol{u} - \boldsymbol{\mu}_u\right)^T \boldsymbol{\Sigma}_u^{-1} \left(\boldsymbol{u} - \boldsymbol{\mu}_u\right) \right), \tag{6}$$

where the mean and covariance of the features are denoted by $\boldsymbol{\mu}_u$ and $\boldsymbol{\Sigma}_u$ respectively. The Gaussian PDF is used because of its simplicity and effectiveness for detecting changes in the features. It is also sensible to use a Gaussian PDF for the features in this dataset as there can potentially be many features and only a few training datasets, which increases the difficulty of estimating the unknown parameters and hyperparameters of complicated models properly.

The naive assumption is made that the features are uncorrelated i.e. the full covariance matrix reduces to a diagonal matrix with the variances of the respective features being on the

diagonal of the covariance matrix. This assumption is made to reduce the number of parameters that need to be estimated from the reference datasets. The mean

$$\mu_u[k] = \frac{1}{N_{train}} \sum_{i=0}^{N_{train}-1} u_{train}^{(i)}[k], \tag{7}$$

and diagonal covariance matrix

$$\Sigma_u[a,k] = \frac{1}{N_{train}-1} \sum_{i=0}^{N_{train}-1} \left(u_{train}^{(i)}[k] - \mu_u[k]\right)^2 \cdot \delta(a-k), \tag{8}$$

of the Gaussian PDF in Equation (6) are obtained from the healthy features, where δ denotes the Kronecker delta function i.e. $\delta(0) = 1$ and 0 otherwise.

The parameters of the model are denoted $\boldsymbol{\Theta} = \{\boldsymbol{\mu}_u, \boldsymbol{\Sigma}_u\}$ and a novelty detection scoring function $\mathcal{M}(u[k]; \boldsymbol{\Theta})$ is used with an associated threshold $\beta_{thres}[k]$ to detect novelties in specific frequency bands i.e. a novelty is detected if $\mathcal{M}(u[k]; \boldsymbol{\Theta}) > \beta_{thres}[k]$. A good novelty detecting scoring function for a Gaussian PDF is the squared Mahalanobis distance which can be simplified to

$$\mathcal{M}(u[k]; \boldsymbol{\Theta}) = \left(\frac{\mu_u[k] - u[k]}{\sqrt{\Sigma_u[k,k]}}\right)^2, \tag{9}$$

for a diagonal covariance matrix.

2.3. Filter design to enhance novel information

It is desired to retain the frequency bands which contain novel information in the novel vibration signal. This is achieved by using the novelty detection score $\mathcal{M}(u[k]; \boldsymbol{\Theta})$ and the associated threshold $\beta_{thres}[k]$ to find the filter coefficient $h[k]$ associated with feature $u[k]$

$$h[k] = \begin{cases} 1.0 & \text{if} \quad \mathcal{M}(u[k]; \boldsymbol{\Theta}) > \beta_{thres}[k], \\ 0.0 & \text{if} \quad \mathcal{M}(u[k]; \boldsymbol{\Theta}) \leq \beta_{thres}[k]. \end{cases} \tag{10}$$

The filter coefficient is equal to unity if a novelty is detected and zero if not. The filter has a similar form to the filter proposed by Combet and Gelman [19], where informative frequency bands are identified and amplified by the square root of the spectral kurtosis. However, in the aforementioned paper, the informative frequency bands were determined from a uniform statistical threshold and did not use historical data in the process. The threshold in Equation (10) is $\beta_{thres}[k] = 9$ for $k = 0, \ldots, N_{feat} - 1$. The motivation for the threshold is that it corresponds to $\mu \pm 3\sigma$ when $\mathcal{M}(u[k]; \boldsymbol{\Theta}) = \beta_{thres}[k]$, which covers 99.7% of the probability density function of a Gaussian distribution.

In Equation (10), it is possible to use a more sophisticated filter as well; for example, if a novelty is detected $h[k] = \mathcal{M}(u[k]; \boldsymbol{\Theta})$ i.e. the novel information is amplified proportionally to its novelty score. However, the binary filter is investigated here to reduce the number of hyperparameters in the model.

2.4. Novel signal estimation

The novel signal is estimated from the novelty filter in two steps. Firstly, each frequency band m of the time-frequency representations of the different window lengths l are scaled by the novelty filter

$$\tilde{S}_x[n, m; \Delta f_l] = h[\kappa(m, l)] \cdot S_x[n, m; \Delta f_l] \tag{11}$$

where $\tilde{S}_x[n, m; \Delta f_l]$ denotes the scaled time-frequency representation $S_x[n, m; \Delta f_l]$. The filter coefficient associated with the centre frequency $m \cdot \Delta f_l$ and decomposition level l is given by $h[\kappa(m, l)]$, where $\kappa(m, l)$ is a function which relates the centre frequency and decomposition level to the index of a filter coefficient. In the second step, the inverse transform of the time-scale distribution at level l, S_x^{-1}, is calculated by the scaled time-frequency representation to obtain an estimation of the novel signal

$$\hat{x}_{novel}[n; \Delta f_l] = S_x^{-1}(\tilde{S}_x[n, m; \Delta f_l]). \tag{12}$$

The $\hat{\cdot}$ makes it explicit that an estimate of the novel signal is obtained. The inverse STFT S_x^{-1} can be used to perfectly reconstruct the signal if constant overlap-add constraint is satisfied [34].

The dependence of the estimation on the frequency resolution Δf_l of the time-frequency decomposition is emphasised in Equation (12). It is ideal to use an estimate that does not depend on the frequency resolution i.e. to use $\hat{x}_{novel}[n]$ instead of $\hat{x}_{novel}[n; \Delta f_l]$. This can be approximated with a weighted sum of the novel signals associated with each decomposition l

$$\hat{x}_{novel}[n] = \sum_{l=0}^{N_l - 1} \hat{x}_{novel}[n; \Delta f_l] \cdot w[l], \tag{13}$$

where $\boldsymbol{w} \in \mathbb{R}^{N_l \times 1}$ denotes the weight vector, which has the following constraint $\sum_{k=0}^{N_l - 1} w[k] = 1$. There are many potential methods to select the elements of the weight vector $\boldsymbol{w}$, with the simplest being to assign an equal weight to each frequency band, which results in

$$\hat{x}_{novel}[n] = \frac{1}{N_l} \sum_{l=0}^{N_l - 1} \hat{x}_{novel}[n; \Delta f_l]. \tag{14}$$

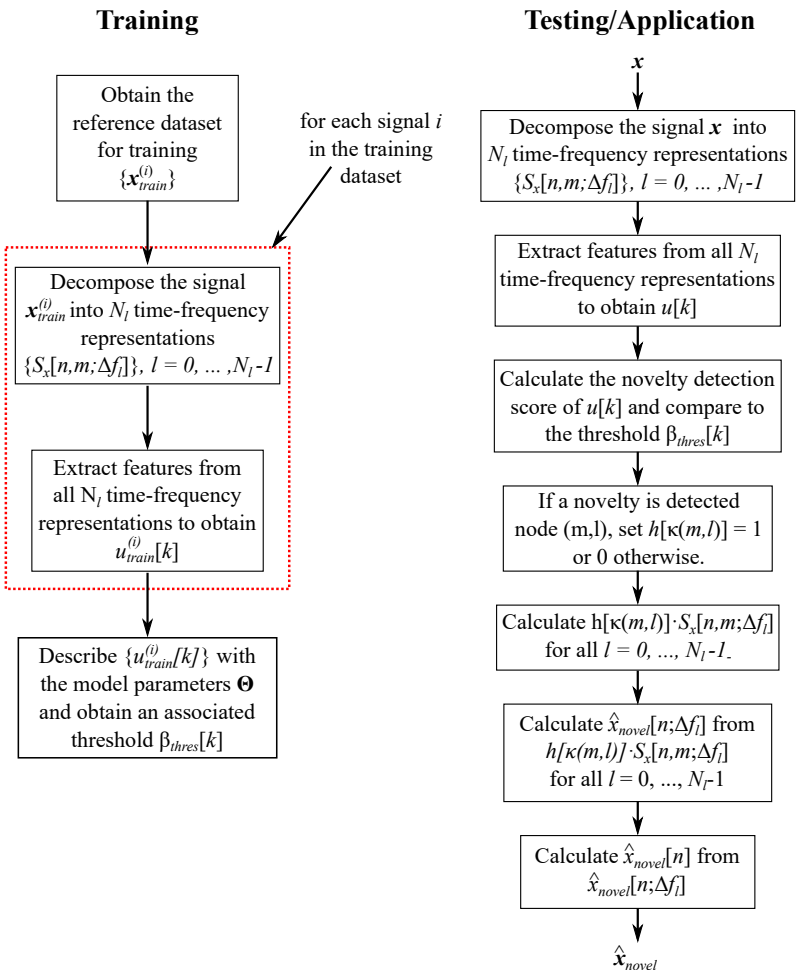

Figure 2: The proposed methodology is illustrated to obtain a novel vibration signal $\hat{\boldsymbol{x}}_{novel}$ from a vibration signal $\boldsymbol{x}$. In the training phase, the reference dataset is used to obtain the model parameters, whereafter a novel signal is extracted from the vibration signal in the testing phase.

Finally, the estimated novel signal can for example be analysed using cyclostationary techniques for the presence of damage in the machine components. Different techniques are investigated for the datasets and described in the following sections.

The methodology, discussed in Section 2.1 to Section 2.4, is summarised in Figure 2 to clarify the steps followed in the training and testing phases.

3. Phenomenological gearbox model

A phenomenological gearbox model is investigated to generate data of a gearbox operating in various machine conditions under constant loads and varying speed conditions. The model is based on the model used by Abboud et al. [12].

3.1. Model

The phenomenological gearbox model is used to generate data in a reference condition, whereafter additional inner and outer race bearing damage is simulated in the gearbox. The gearbox signal in its reference condition consists of a gear mesh component x_{gmc}, a noise component x_n and a distributed gear damage component x_{dgd}, with the corresponding casing vibration signal given by

$$x_c(t) = x_{gmc}(t) + x_{dgd}(t) + x_n(t). \tag{15}$$

The condition of the gearbox in its reference condition is changed by introducing localised outer race damage $x_{blo}(t)$ and localised inner race damage $x_{bli}(t)$ with the updated casing vibration signal given by

$$x_c(t) = x_{gmc}(t) + x_{dgd}(t) + FS_{blo} \cdot x_{blo}(t) + FS_{bli} \cdot x_{bli}(t) + x_n(t). \tag{16}$$

The fault severity factors FS_i help to explicitly change the magnitude of the bearing damage components with respect to the other signal components e.g. $FS_i = 0$ indicates that the associated signal component is not present in the signal.

The gear mesh component of the gearbox

$$x_{gmc}(t) = M\left(\omega(t)\right) \cdot h_{gmc}(t) \otimes \left(\sum_{k=1}^{N_{gmc}} A_{gmc}^{(i)} \cdot \sin\left(k \cdot N_{teeth} \cdot \int_0^t \omega(\tau) d\tau + \varphi_{gmc}^{(k)} \right) \right), \tag{17}$$

consists of a component that alters the magnitude of the signal as the rotational speed ω[rad/s] changes i.e. $M\left(\omega(t)\right)$, while $A_{gmc}^{(k)}$ and $\varphi_{gmc}^{(k)}$ are the magnitude and phase of the kth harmonic component of the N_{gmc} gear mesh components. The single degree-of-freedom impulse response function of the gear mesh component is denoted as $h_{gmc}(t)$. The number of teeth on the gear connected to the reference shaft is denoted by N_{teeth}, where the instantaneous gear mesh frequency in rad/s is given by $N_{teeth} \cdot \omega(t)$.

The distributed gear damage component

$$x_{dgd}(t) = M(\omega(t)) \cdot h_{dgd} \otimes \left(\varepsilon_\sigma(t) \cdot \sum_{k=1}^{N_{dgd}} A_{dgd}^{(k)} \cdot \sin\left(k \cdot \int_0^t \omega(\tau) d\tau + \varphi_{dgd}^{(k)} \right) \right), \tag{18}$$

has a similar form as the gear mesh component in Equation (17); the only differences are the random sample from a zero mean Gaussian distribution with unit variance denoted by $\varepsilon_\sigma(t)$ and the fundamental frequency of the distributed gear damage that is associated with the rotational speed of the shaft as opposed to the gear mesh frequency.

The outer race bearing damage component

$$x_{blo}(t) = M(\omega(t)) \cdot h_{blo}(t) \otimes \left(\sum_{k=0}^{N_{imp}} A_{blo}^{(k)} \cdot \delta \left(t - T_{blo}^{(k)} \right) \right), \tag{19}$$

consists of a train of Dirac impulses δ convolved with the impulse response function $h_{blo}(t)$. The impulses are random in magnitude, captured by the random variable $A_{blo}^{(k)}$, and are modulated by the rotational speed of the system with the function $M(\omega(t))$ as well. The time-of-arrival of bearing impulse k, denoted by $T_{blo}^{(k)}$, is influenced by the rotational speed of the system as well as by slip [10]. Hence, the instantaneous phase of the shaft is used to relate the angle and time of the impulses whereafter slippage effects are introduced by adding noise from a uniform distribution to the time of arrival of the impulses.

The inner race damage component

$$x_{bli}(t) = z_{stribeck} \left(\int_0^t \omega(\tau) d\tau \right) \cdot M(\omega(t)) \cdot h_{bli} \otimes \left(\sum_{k=0}^{N_{imp}} A_{bli}^{(k)} \cdot \delta \left(t - T_{bli}^{(k)} \right) \right), \tag{20}$$

has a similar form as the outer race component, except for the presence of the Stribeck equation [35]

$$z_{stribeck}(\varphi) = \begin{cases} z_0 \cdot \left(1 - \frac{1}{2\epsilon} \left(1 - \cos(\varphi)\right)\right)^{c_{str}} & \text{for } |\text{wrp}(\varphi)| < \varphi_{max} \\ 0 & \text{otherwise,} \end{cases} \tag{21}$$

which simulates the damaged portion of the inner ring moving in-and-out of the load zone. The wrap function, denoted by $\text{wrp}(\varphi)$, returns the phase of the shaft φ in the domain of $[-\pi,\ \pi]$. The constants associated with the Stribeck equation is selected as [35]: $c_{str} = 3/2$, $\epsilon = 0.49$, $\varphi_{max} = 0.99\pi/2\text{rad}$, and $z_0 = 1$.

The last component of the casing vibration signal is the noise signal

$$x_n(t) = \sigma_n \cdot \varepsilon_\sigma(t) \cdot M(\omega(t)), \tag{22}$$

which contains a sample from a zero mean, unit variance Gaussian function $\epsilon_\sigma(t)$, which is scaled by a constant factor σ_n and with the function $M(\omega(t))$. The dependence of each vibration component on the rotational speed of the system is governed by the same function $M(\omega(t)) = \omega^2$ for the sake of simplicity.

An overview of the parameters used in the dataset is given in Appendix A, with the vibration signals presented as well. However, it is important to highlight the model characteristics that assist with interpreting the results; the ball-pass outer race and inner race orders of the bearing are 4.12 and 5.88, while, the natural frequencies being excited by the outer race damage and inner race damage are 7.0 kHz and 5.5 kHz, respectively.

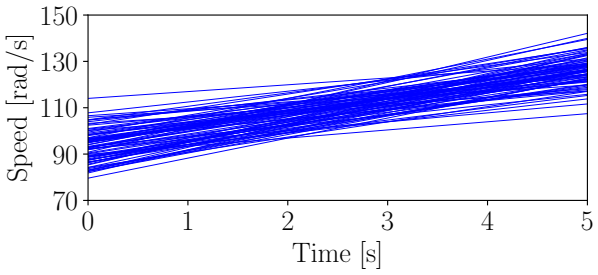

Figure 3: The rotational speeds used for the phenomenological gearbox model are presented, with the rotational speed associated with a specific measurement obtained from $\omega(t) = at + b$. The parameters a and b are sampled from a normal distribution with unit variance, with $\mathbb{E}\{\omega(t)\} = 10\pi \cdot t + 30\pi$ rad/s.

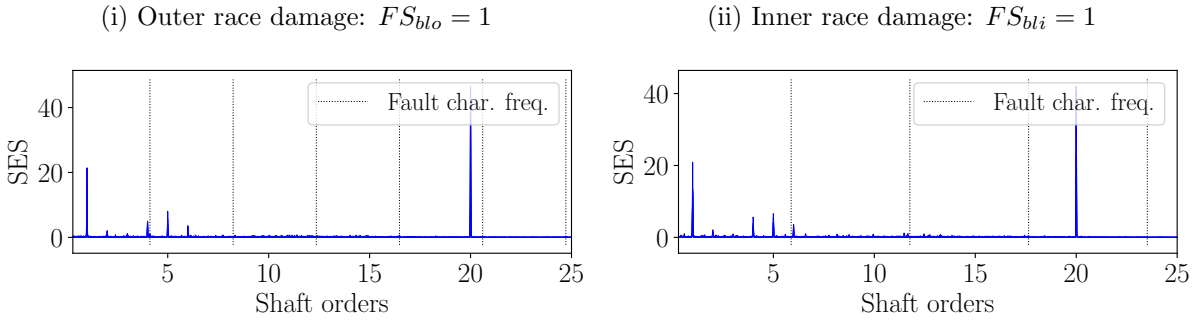

Figure 4: The Squared Envelope Spectrum (SES) of the original casing vibration signal from the phenomenological gearbox model that contains outer race bearing damage and inner race damage, are presented. The analytical fault frequencies and their harmonics are superimposed on the spectra as well.

The rotational speeds for all casing vibration signals are linear ramp-ups, with the initial rotational speed and the gradient determined from a normal distribution. The random rotational speed profiles are presented in Figure 3.

3.2. Results with raw data

The Squared Envelope Spectrum (SES) is one of the most powerful tools in bearing diagnostics [12] and therefore it is investigated on the casing vibration signals. In Figure 4(i), the SES is presented of the raw vibration signal, which corresponds to the bearing with outer race damage. In Figure 4(ii), the SES of the raw vibrations signal, which corresponds to the bearing with inner race damage is presented. The distributed gear damage manifests at the shaft orders and their harmonics are clearly seen, while the gear mesh component is prominent at 20 shaft orders. The bearing damage signal components' are not seen in Figure 4 for both cases. Usually, the SES of the random part is calculated i.e. where the deterministic components such as the

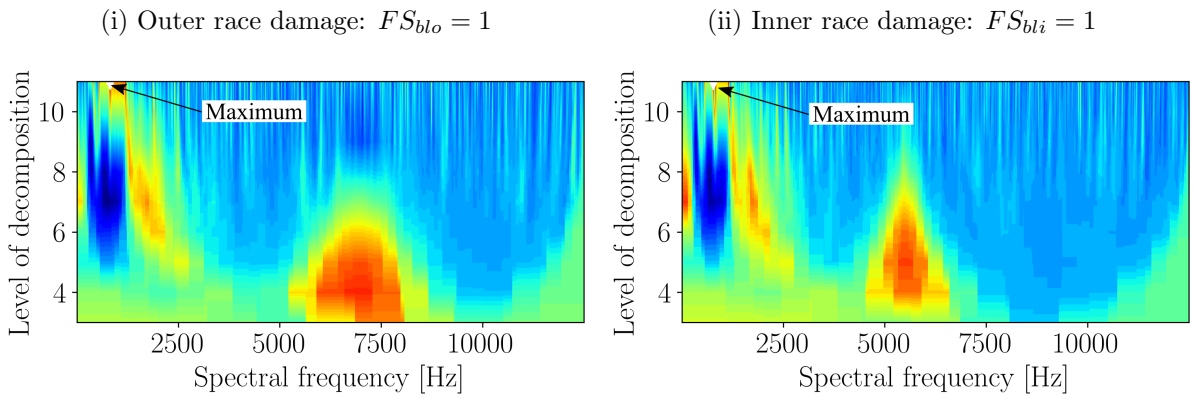

Figure 5: The squared envelope infogram of the raw casing vibration signal of the phenomenological gearbox model that contains outer race and inner race damage respectively, is presented. The infogram in Figure 5(i) corresponds to the SES in Figure 4(i) and the infogram in Figure 5(ii) corresponds to the SES in Figure 4(ii).

gear mesh components are attenuated [36], but the distributed gear damage will not be removed due to the statistical nature of its characteristics i.e. it is second-order cyclo-non-stationary. The complete signal, as opposed to the residual signal, is used in all analyses to illustrate the ability of the proposed methodology to remove the healthy characteristics from the data.

It is possible to design a bandpass filter by selecting the centre frequency band and the frequency resolution that maximise the SE infogram shown in Figure 5(i) for the outer race damage and in Figure 5(ii) for the inner race damage. However, the distributed gear damage signal components dominate the feature plane which results in the wrong bandpass filter to be designed i.e. the resulting bandlimited signal only contains the distributed gear damage information. Hence, it is sensible to use the proposed methodology to incorporate the information of the historical data of the machine in a reference condition into the signal analysis procedure to assist with diagnosing the gearbox. The proposed methodology is investigated in the next section.

3.3. Results with proposed methodology

Twenty datasets of the gearbox in its reference condition are generated with Equation (15) and used in the training phase of the methodology. The squared envelope infogram given by Equation (4) is used as the features in this investigation, however other features could also be investigated as alternatives as discussed in Section 2.1. The model parameters are obtained from the features of the reference dataset using the procedure described in Section 2.2.

In the testing phase, the vibration data of the phenomenological gearbox model that contains

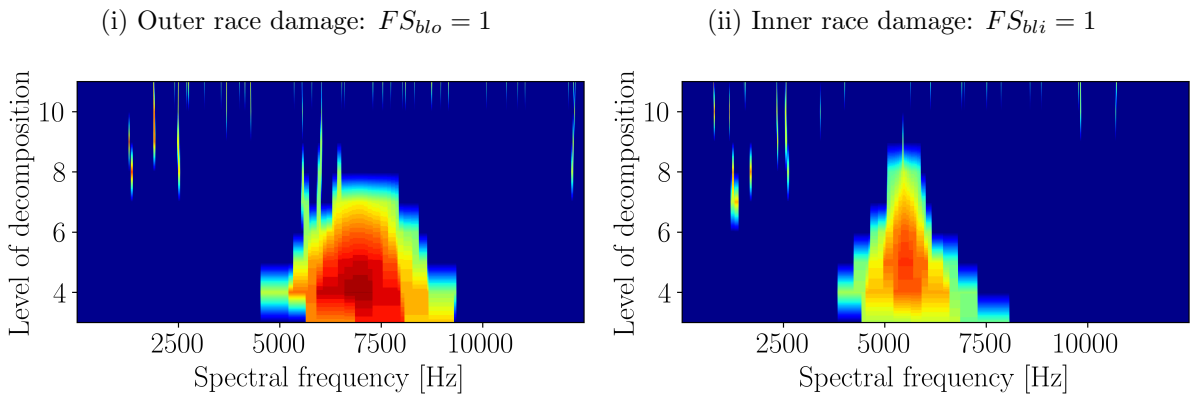

Figure 6: The squared envelope infogram of the estimated novel signal of the phenomenological gearbox model that contains outer race and inner race damage respectively, is presented. The raw signal counterpart of Figure 5(i) is presented in Figure 6(i), while the raw signal counterpart of Figure 5(ii) is presented in Figure 6(ii).

either inner race or outer race damage are considered. Different magnitudes of the signal components associated with the damaged bearing are investigated by changing FS_i in Equation (16). This is performed to ensure that it is possible to not only detect and localise the bearing damage, but that it is also possible to infer changes in the condition of the bearing. The methodology is applied on the datasets by using the same feature extraction procedure, whereafter the model is used to assign a novelty score to each feature in the feature map with Equation (9). This is used with the threshold to design the filter given by Equation (10), whereafter the estimated novel signal is obtained with the procedure described in Section 2.4.

The squared envelope infogram is presented in Figure 6 for the novel signals corresponding to the squared envelope infogram in Figure 5. It is evident that the bearing damage located in the higher frequency bands are retained in the filtering process, while the distributed gear damage components are not dominating the feature plane any longer. It is also observed that some spurious frequency bands are retained in the higher decomposition levels. This is possibly attributed to the statistics being improperly estimated due to the poor time resolution. However, with the averaging approach in Equation (14), the effect of the spurious components is attenuated.

The SES of the novel signals are presented in Figure 7. A significant improvement is observed in Figure 7 compared to the results in Figure 4 for a $FS_i = 1$. The bearing fault frequencies and the associated modulations are prominent in the spectra of the novel signals, which is in contrast to the SES of the raw signals where the distributed gear damage and the fundamental gear mesh frequency dominated the lower frequency range of the spectrum. The squared envelope spectra

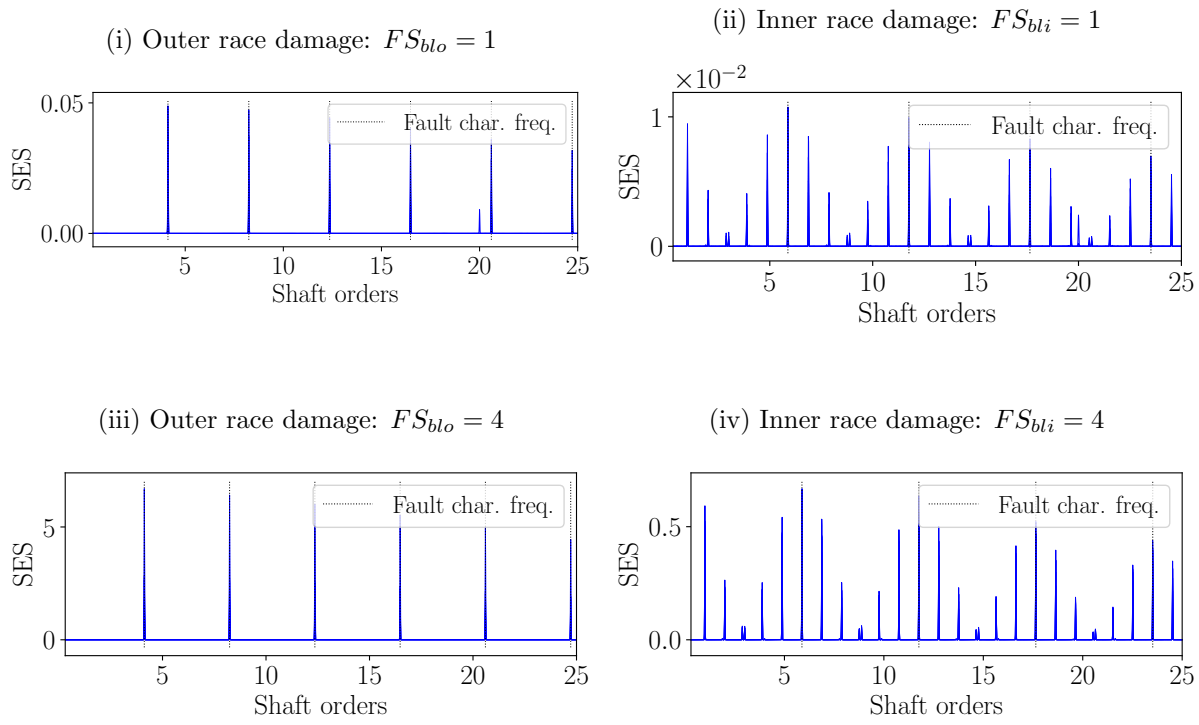

Figure 7: The Squared Envelope Spectrum (SES) of the novel vibration signals for different levels of outer race and inner race bearing damage are shown.

in Figure 7 also indicate that changes in the condition of the bearings can be detected i.e. an increase in FS_i results in an increase in the amplitudes of the fault components.

The vibration signals are cyclo-non-stationary under varying speed conditions, while the bearing vibration signal can be approximated as an angle-time cyclostationary signal. This makes the Order-Frequency Spectral Correlation (OFSC) [7]

$$\mathrm{SC}(\alpha_\theta, f) = \lim_{T\to\infty} \frac{1}{\theta(T)} \mathbb{E}\left\{ \mathcal{F}_T\left(x(t)\right)^* \mathcal{F}_T\left(x(t)e^{-j\alpha_\theta \theta(t)}\omega(t)\right)\right\}, \tag{23}$$

a powerful tool for analysing the vibration signals. The spectral correlation in Equation (23) is defined over the cyclic order α_θ and spectral frequency f for a continuous signal of time $x(t)$, where T is the time duration of the signal. The instantaneous phase of the shaft in radians is given by $\theta(t) = \int_0^t \omega(\tau)d\tau$. The Fourier transform of a continuous function is defined as $\mathcal{F}_T(\cdot)$ and $\mathbb{E}$ is the expectation operator. The OFSC is estimated with the Averaged Cyclic Periodogram (ACP) for the considered discrete signals [7].

The spectral correlation is presented for a bearing with outer race damage in Figure 8(i) and Figure 8(ii) for the original and estimated novel signals respectively. As opposed to the results in Figure 8(i) that are dominated by the gear components at 20 shaft orders, the bearing damage can be seen at the spectral frequency of 7 kHz, spaced at cyclic orders of 4.12 in Figure 8(ii).

The Enhanced Envelope Spectrum (EES), estimated with the Spectral Correlation (SC)

$$\mathrm{EES}_{\mathrm{SC}}(\alpha_\theta) = \int |\mathrm{SC}(\alpha_\theta, f)| df \tag{24}$$

highlights the spectral frequency components that are present in the OFSC and is presented in Figure 8(iii) and Figure 8(iv) for the spectral correlation of the original and novel signals investigated in Figure 8(i) and Figure 8(ii). The $\mathrm{EES}_{\mathrm{SC}}$ of the original vibration signal is dominated by the distributed damage and the gear mesh component, while the $\mathrm{EES}_{\mathrm{SC}}$ of the novel vibration signal is similar to the results seen in the squared envelope spectrum in Figure 7(iii). Hence, by using the estimated novel vibration signal of the vibration signal, the novel information associated with the bearing damage is highlighted, while the historical information is attenuated. Similar conclusions were drawn from the inner race damage signal results and therefore the results are excluded for the sake of brevity.

The Order-Frequency Spectral Coherence (OFSCoh) is another useful quantity for analysing second-order cyclo-non-stationary signals. The OFSCoh [36]

$$\gamma(\alpha_t, f) = \frac{\mathrm{SC}(\alpha_t, f)}{\left(\mathrm{SC}(0, f)\mathrm{SC}(0, f+\alpha_t)\right)^{1/2}}, \tag{25}$$

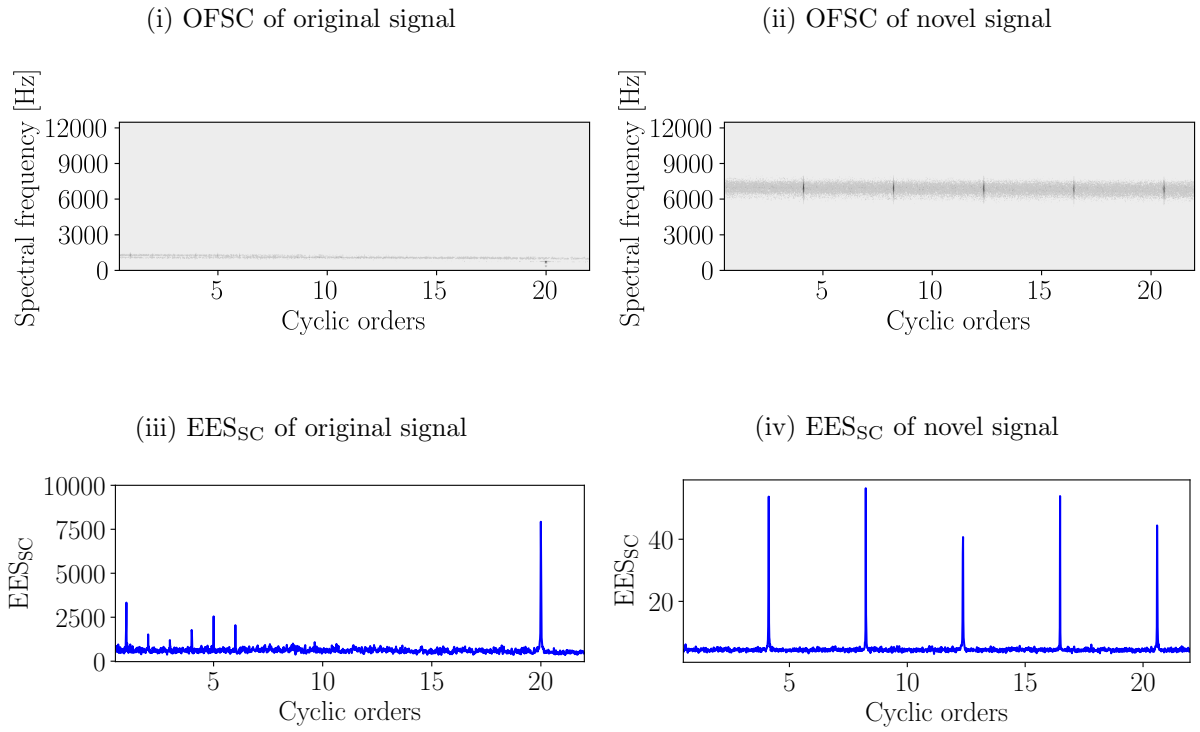

Figure 8: The magnitude of the spectral correlation of the gearbox with outer race damage is presented in Figure 8(i) for the original signal and 8(ii) for the estimated novel signal. The corresponding Enhanced Envelope Spectrum based on the Spectral Correlation EES$_{SC}$ is shown in Figure 8(iii) for the original signal and Figure 8(iv) for the novel signals.

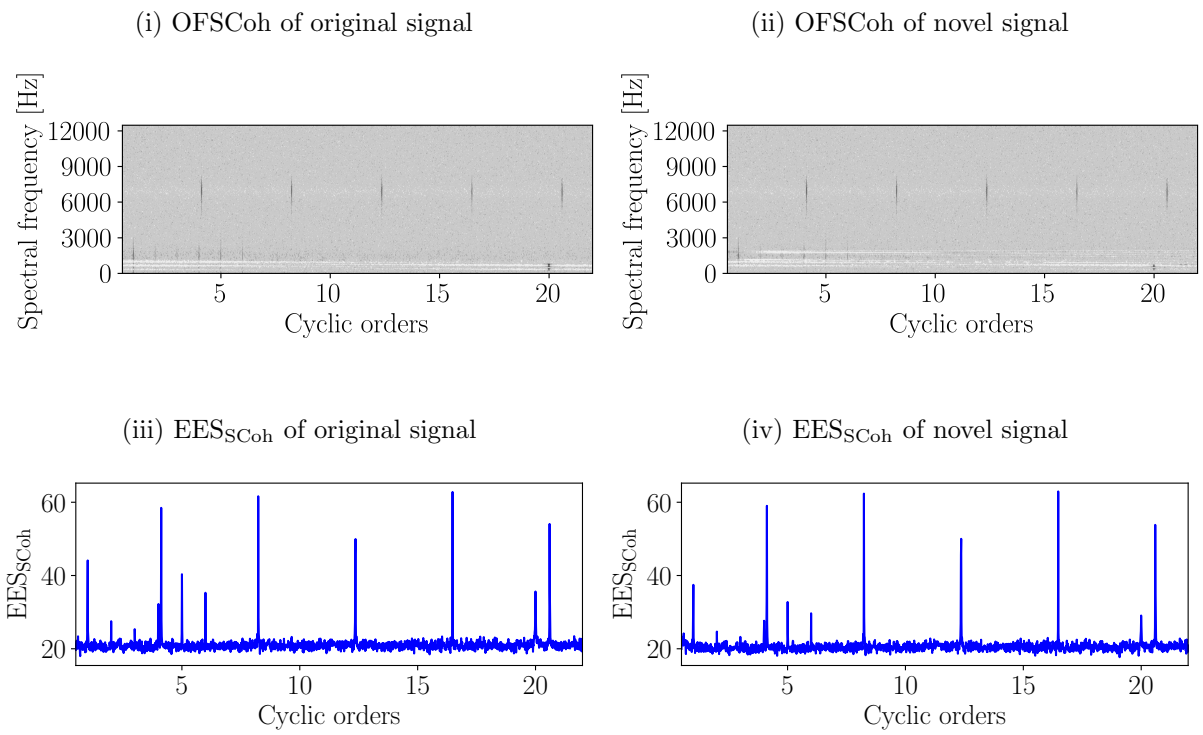

Figure 9: The magnitude of the Order-Frequency Spectral Coherence (OFSCoh) is shown for the original signal with outer race damage in Figure 9(i) and the estimated novel signal in Figure 9(ii). This corresponds to the Order-Frequency Spectral Correlation (OFSC) in Figure 8(i) and Figure 8(ii). The Enhanced Envelope Spectrum (EES$_{\text{SCoh}}$) is shown in Figure 9(iii) for the OFSCoh in Figure 9(i) and the EES is shown in Figure 9(iv) for the OFSCoh in Figure 9(ii).

is a normalised representation of the SC, which helps to amplify small second-order components. The Enhanced Envelope Spectrum (EES$_{\text{SCoh}}$) based on the Spectral Coherence (SCoh) [37]

$$\text{EES}_{\text{SCoh}}(\alpha_t) = \int |\gamma(\alpha_t, f)| df \tag{26}$$

is calculated from the OFSCoh and is another useful quantity to detect small second-order cyclostationary components. The OFSCoh is presented in Figure 9(i) and Figure 9(ii) for the original and the estimated novel vibration signals also investigated in Figure 8. The attenuated gear components are more prominent in the OFSCoh as opposed to the OFSC. This is attributed to the fact that the OFSCoh enhances small signal components, which is also verified by the EES$_{\text{SCoh}}$ of the signals, which shows that the attenuated gear components are enhanced. The bearing damage is more prominent with respect to the gear components in Figure 9(iv) than in Figure 9(iii). This illustrates two important points that while the OFSCoh and the EES$_{\text{SCoh}}$ are very powerful and important for detecting small second-order cyclostationary components in

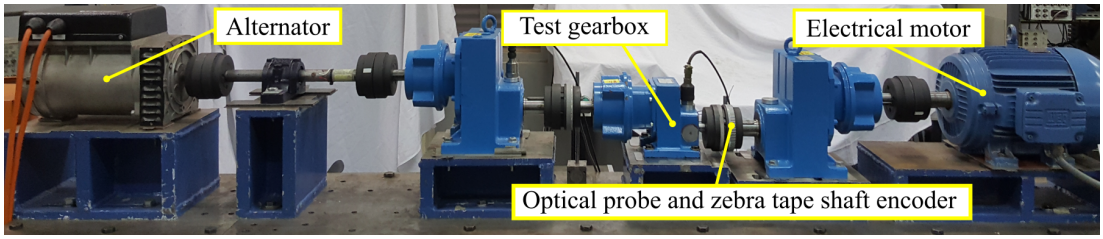

Figure 10: The experimental setup used to generate the experimental gearbox dataset.

vibration signals, these techniques do not accurately convey the novel information content of the vibration signal (i.e. they amplify the information that was previously attenuated).

The results in this investigation illustrate the potential of the proposed methodology. It is possible to attenuate the historical information from different interfering sources, which results in the novel damage information to be enhanced. The implication is that non-diagnostic frequency bands that dominate the signal and impede the fault diagnosis process, are automatically attenuated based on a statistical criterion.

4. Experimental gearbox dataset

4.1. Experimental setup

The experimental gearbox dataset was acquired from a gearbox setup in the Centre for Asset Integrity Management laboratory at the University of Pretoria. The gearbox setup presented in Figure 10 consists of three gearboxes, an electrical motor which can be controlled with a personal computer to induce varying speed conditions and an alternator which can be controlled to apply varying loads to the system. The test gearbox in a healthy condition was used to collect vibration data for the reference dataset, whereafter the test gearbox was disassembled, a gear tooth was damaged and the test gearbox was reassembled with the damaged gear. The gearbox was damaged by seeding a slot in a single tooth of the gear, whereafter the gearbox was operated until the gear tooth ultimately failed.

The gear of the test gearbox with the damaged gear tooth in its initial condition and the same gear in its final condition are presented in Figure 11. A hundred measurements between the two conditions in Figure 11 are used in the investigations. The actual condition of the gear was only known for the first measurement and the last measurement. This is because the condition of the gears could only be inspected by disassembling the gearbox, which would have compromised the integrity of the data if performed during the fatigue experiments.

(i) Before (ii) After

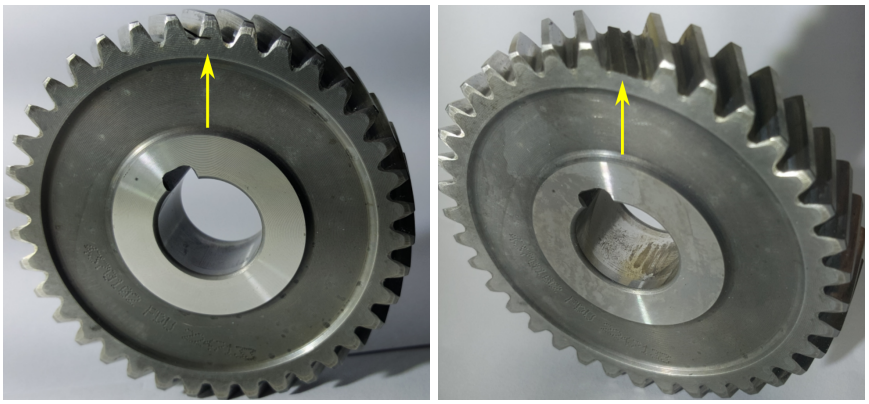

Figure 11: The damaged gear in its initial condition before the experiment started and the damaged gear after the experiment was completed are presented in Figure 11(i) and Figure 11(ii), respectively.

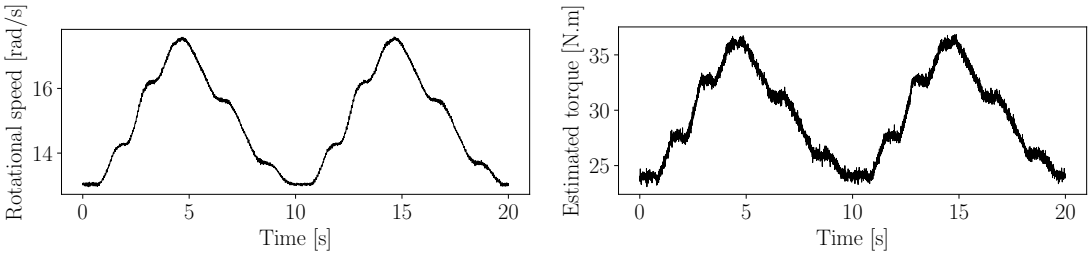

Figure 12: The operating conditions i.e. load and speed, present at the input shaft of the test gearbox, are presented.

The operating conditions that were present when the healthy and the damaged datasets were acquired are presented in Figure 12.

The axial component of a tri-axial accelerometer located on the bearing housing of the test gearbox is used in this investigation. The spectrogram of the vibration signal of the gearbox with localised gear damage is presented in Figure 13(i) where the vertical lines indicate the approximate spectral frequencies where the gear damage can be observed. The time varying frequency components, attributed to the gear mesh interactions, are proportional to the rotational speed of the input shaft presented in Figure 12, and clearly seen throughout the spectrogram of the signal. The time invariant frequency components are also clearly seen.

The benefit of using features of narrowband signals as opposed to calculating the difference between spectra is illustrated in Figure 13(ii), with the vertical lines being used to make the comparison easier between the two plots in Figure 13(ii) and the spectrogram in Figure 13(i). It is evident that the largest value for ΔSE negentropy between the SE negentropy of the damaged

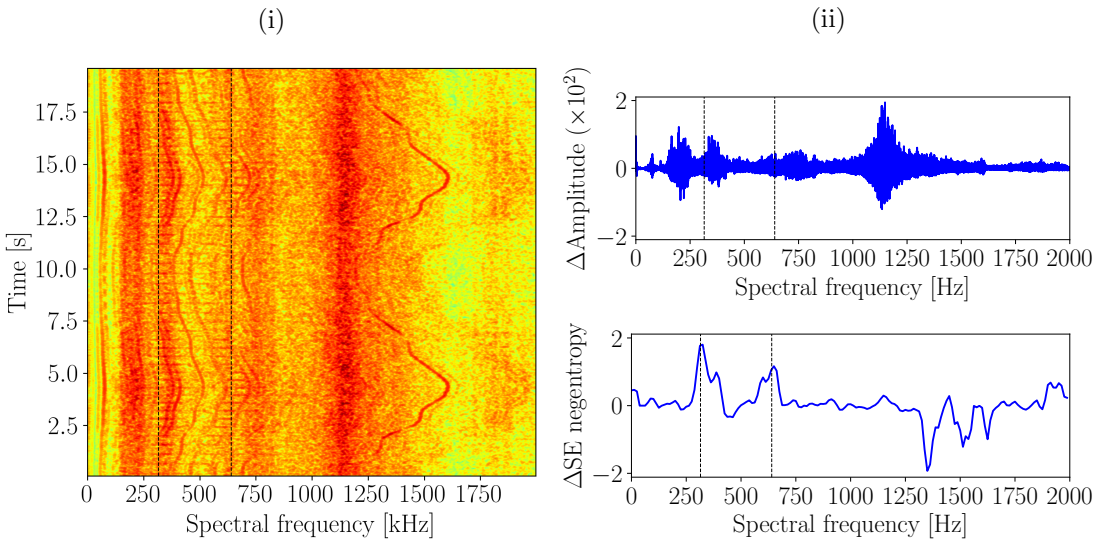

Figure 13: The spectrogram of a gearbox with localised damage under variable operating conditions is presented in Figure 13(i). The benefits for using the statistics of narrowband signals (in this case the spectral negentropy) as opposed to the amplitudes of the frequency components for detecting frequency bands with novel information are illustrated in Figure 13(ii).

gearbox signal and the averaged SE negentropy of the healthy gearbox signals occurs in the frequency bands where the damage is observed in Figure 13(i) i.e. they are highlighted with the vertical lines. This is in contrast to the results of Δ Amplitude; the amplitude difference is very sensitive to the operating conditions and the time-invariant frequency content seen at approximately 1100Hz. This supports using features, extracted from bandlimited signals, in the methodology as opposed to differences in spectra for designing the novel filter.

The methodology is further motivated by:

- The damage results in significant changes in the SE negentropy in two distinct frequency bands in Figure 13(ii) as indicated by the vertical lines. This emphasises that more than one frequency band can potentially be used for demodulation for example. This is contrast to the methods in literature where only a single frequency band is selected for further analyses.

- The ΔSE infogram in Figure 13(ii) can be difficult to interpret manually, especially if many window lengths are investigated for the STFT decomposition, which is why an automatic statistical approach to incorporate the information of the different frequency bands into a single signal which can be used for further analyses, is required.

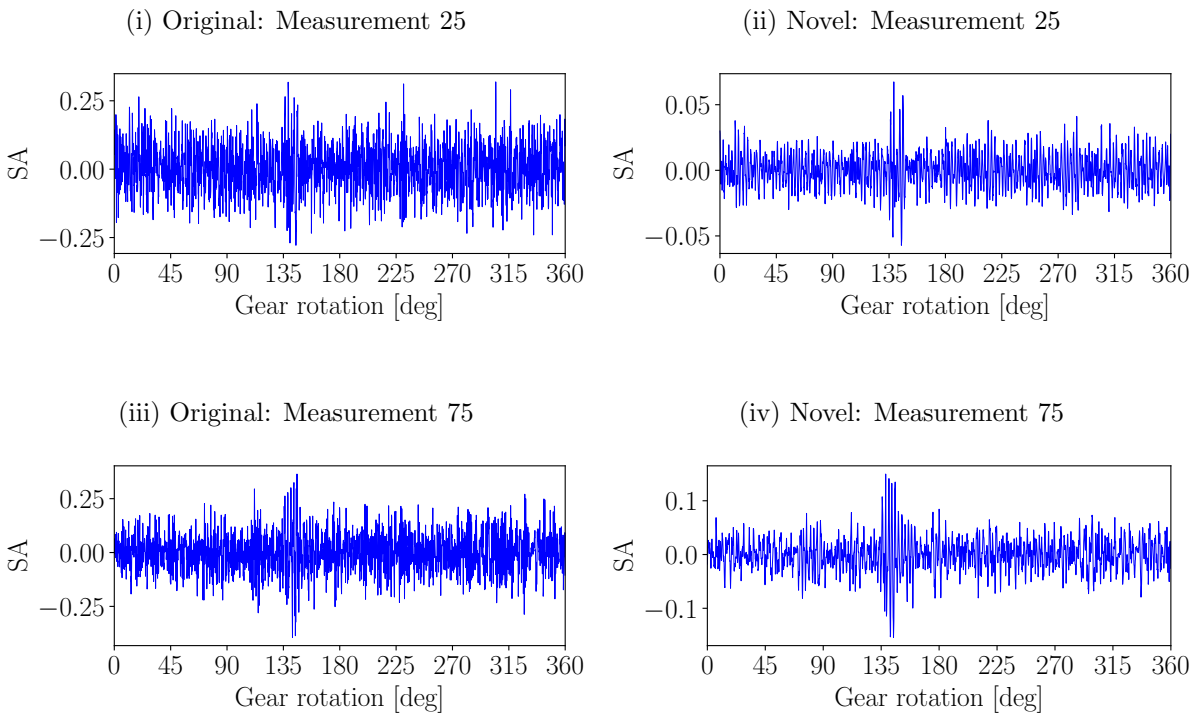

Figure 14: The synchronous averages of two measurements of the damaged gear dataset are presented.

4.2. Results

The proposed methodology is implemented as in the previous datasets. The SE infogram is used as features for consistency, whereafter a Gaussian model is used to describe the model parameters of the healthy dataset. The healthy dataset consists of 30 measurements. The novel information filter is designed using the proposed procedure and compared to the original signal using different signal processing techniques for different measurements.

4.2.1. Results with conventional methods

A popular signal analysis technique for gear diagnosis is the synchronous average of the vibration signal [38, 39]. The synchronous average is adversely affected by the modulation induced by varying operating conditions, but the load and speed variations are non-synchronous with respect to the shaft rotations and their influence are attenuated by the synchronous averaging process [39].

The synchronous averages for an original vibration signal and the corresponding novel vibration signal are presented for two measurements in Figure 14. Note that a total of 100 measurements are used between the two gear conditions shown in Figure 11, e.g. Measurement 75

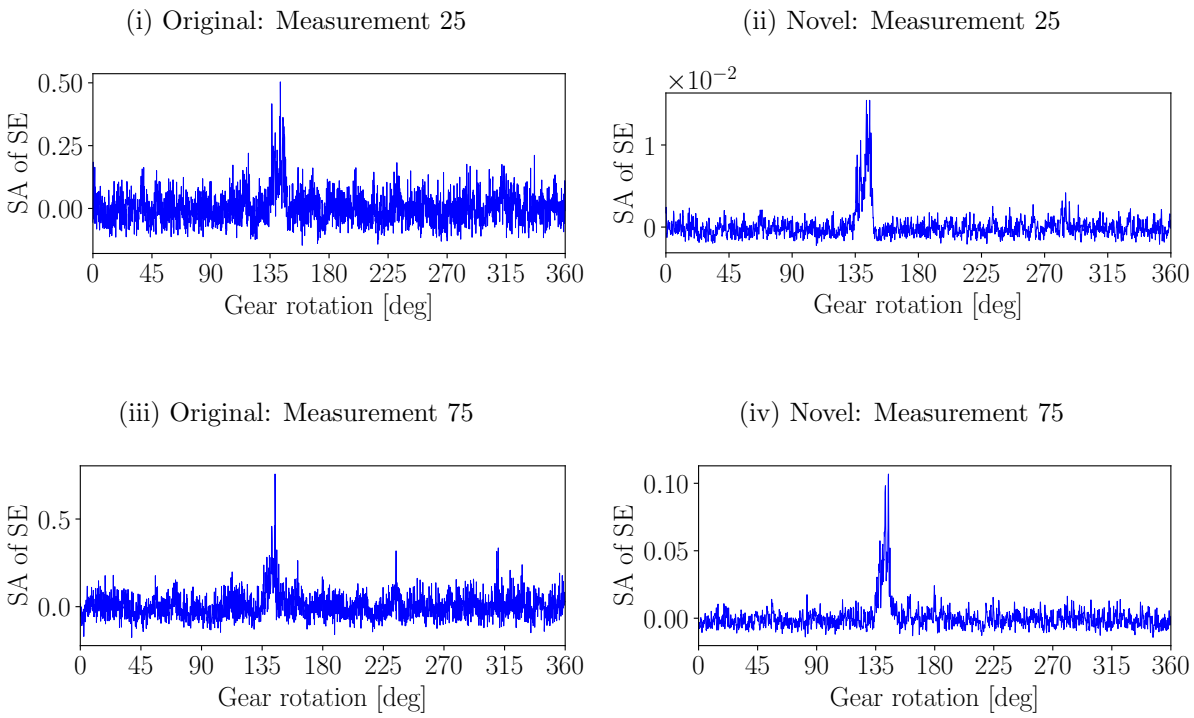

Figure 15: The synchronous averages of the squared envelope of two measurements of the damaged gear dataset are presented.

means that 75% of the experimental time has elapsed. The gear damage was less developed for the measurement used in Figures 14(i) and 14(ii) compared to the measurement used in Figures 14(iii) and 14(iv) which resulted in vibration signals with larger amplitudes in the latter results for the novel signal. This is not evident in the original signal. Even though the synchronous averages of the raw vibration signals in Figure 14(i) and Figure 14(iii) do not clearly highlight the fact that only localised gear damage at approximately 135 degrees is present, the results are improved when calculating the synchronous average of the novel vibration signals shown in Figure 14(ii) and Figure 14(iv). In the novel vibration results, the damage component is more prominent with fewer spurious impulses that impede the condition inference process.

The squared envelope of the vibration signal indicates the instantaneous power of the vibration signal over time and can highlight potential impulses induced by damage. The localised gear damage results in periodical, localised changes in the power of the vibration signal and therefore the synchronous average of the squared envelope is investigated as well. The synchronous averages of the square envelope corresponding to the signals in Figure 14 are presented in Figure 15. It is evident from the results that the synchronous average of the instantaneous power highlights

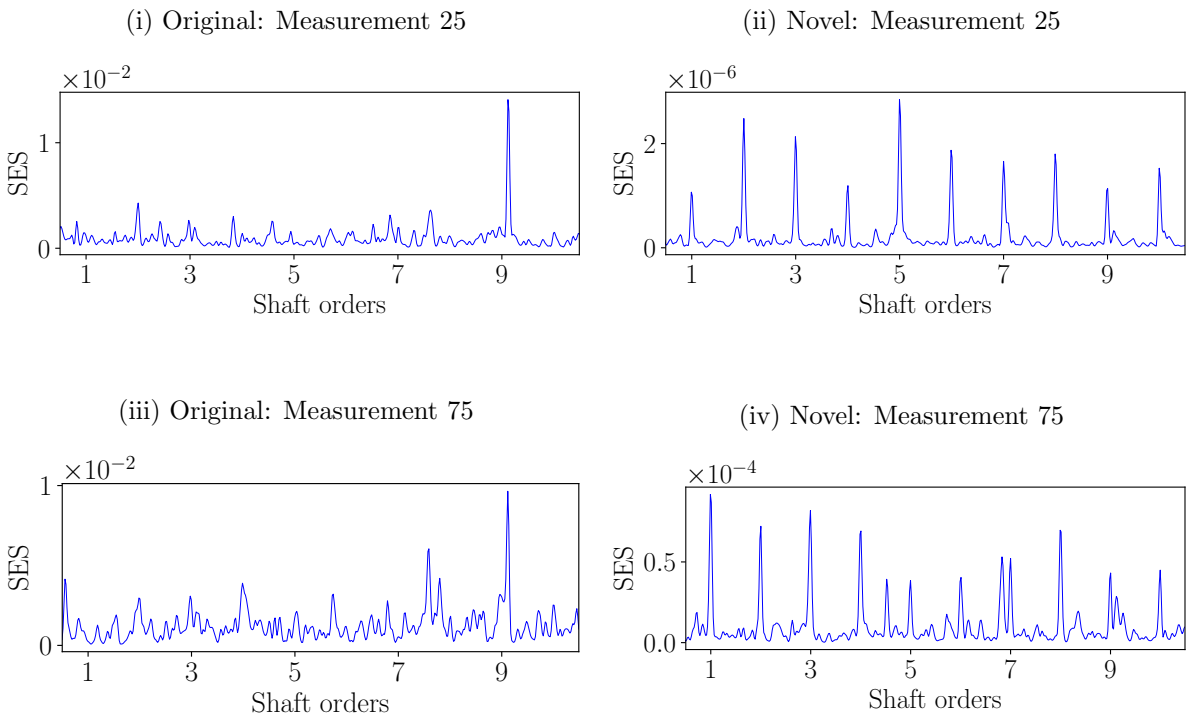

Figure 16: The Squared Envelope Spectrum (SES) is presented for the damaged gearbox data, with different y-axis scales being used. The SES presented in this figure corresponds to the results in Figure 15.

the localised damage better for the original and the novel cases as opposed to the synchronous average of the vibration signals. However, a significant improvement is seen in the novel vibration signals' results in Figure 15(ii) and Figure 15(iv) when compared to the corresponding original vibration signals' results in Figure 15(i) and Figure 15(iii). This highlights that the proposed pre-processing methodology is capable of highlighting the diagnostic information better and it also leads to results that are easier to analyse.

The SES is also investigated and presented in Figure 16 for the different signals being considered. Even though the SES is useful for characterising pure second-order cyclostationary signals, it is useful to quantify periodic changes in the instantaneous power of the vibration signal induced by the localised gear damage. The damaged gear is located on the shaft with the zebra tape shaft encoder and therefore the damage occurs at one shaft order and its harmonics. It is evident from the results in Figure 16(i) and Figure 16(iii) that the modulation induced by the localised gear damage is not prevalent in the original vibration signal. The signal component at 9.12 shaft orders is attributed to the shaft at the alternator being slightly unbalanced. This is in contrast to the SES of the novel vibration signals in Figure 16(ii) and Figure 16(iii). The signal

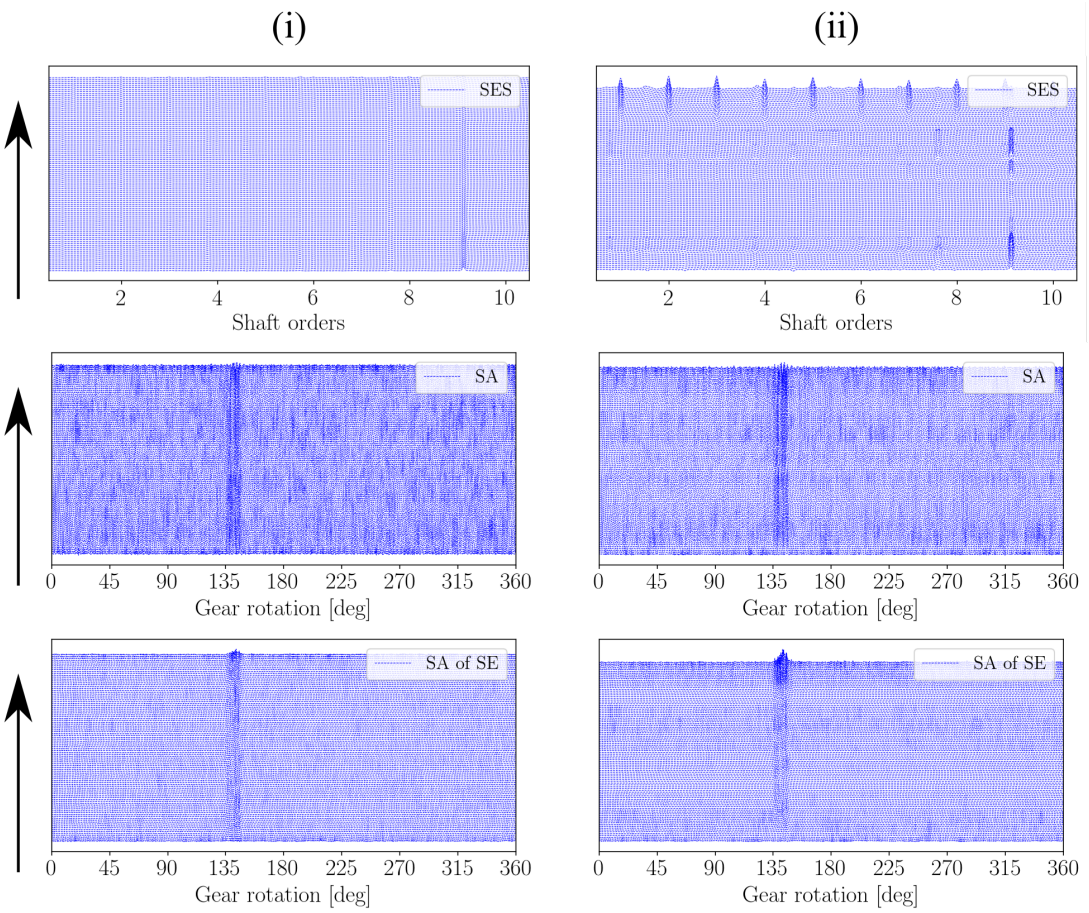

Figure 17: The waterfall plots of the smoothed Synchronous Average (SA) of the vibration signals, the smoothed Synchronous Average of the Squared Envelope (SA of SE) of the vibration signals and the smoothed Squared Envelope Spectrum (SES) are presented. The arrow indicates an increase in measurement number.

components at the shaft harmonics due to the gear damage are clearly visible and dominate the SES. This further validates that the novel vibration signal highlights the diagnostic information in the vibration signal, with the periodicity of the damage clearly detected.

It is reassuring to show that the results presented in Figures 14, 15 and 16 were not obtained by cherry picking and therefore the results are presented for all measurements used in this investigation. The results for the 100 damaged measurements, spaced throughout the life of the damaged gear i.e. from Figure 11(i) to Figure 11(ii), are presented in Figure 17. The results in Figure 17 are obtained by adding a vertical offset to each measurement, with the offset increasing linearly with measurement number. It is clear from the results of the smoothed synchronous averages of the squared envelope i.e. SA of SE and the smoothed SES, that the novel signal is more sensitive to damage. The damage component and the change in the severity of the damage component in the final stages of the gears' life are very prominent when compared

to the original signal. The smoothing, calculated from a second averaging process suggested by [40], is permissible for data acquired over a long time and is used to remove spurious noise which makes the results difficult to interrogate.

4.2.2. Quantification of performance

It is difficult to compare the performance of the methodology to the raw signal from Figure 17. Therefore, it is advantageous to use quantitative measures as basis of comparison and therefore three performance metrics are used on this dataset. The first metric is the kurtosis of the vibration signal $\boldsymbol{x} \in \mathbb{R}^{N_x}$

$$\text{kurtosis}(\boldsymbol{x}) = \frac{\frac{1}{N_x}\sum_{i=1}^{N_x}\left(x[i]-\bar{x}\right)^4}{\left(\frac{1}{N_x}\sum_{i=1}^{N_x}\left(x[i]-\bar{x}\right)^2\right)^2} - 3, \tag{27}$$

which is popular for incipient fault detection. In Equation (27), the mean of the vibration data $\boldsymbol{x}$ is denoted by $\bar{x}$. The kurtosis, as defined in Equation (27), is zero for Gaussian data and increases as the tails of the distribution increase e.g. as the impulsiveness of the dataset increase.

The second metric under consideration is the Quality Measure (QM) of the SES and given by

$$\text{QM}_{\text{SES}} = 10\log\left(\frac{\text{SES}_{damaged}\left(\boldsymbol{x}\right)}{\text{SES}_{noise}\left(\boldsymbol{x}\right)}\right). \tag{28}$$

In Equation (28), $\text{SES}_{damaged}(\boldsymbol{x})$ denotes the average of the damage components in the SES and $\text{SES}_{noise}(\boldsymbol{x})$ is an estimate of the noise floor of the SES. Hence, it is desired to obtain a SES which maximises the QM for the SES i.e. QM_{SES}. The calculation procedure is illustrated in Figure B.1 in Appendix B.

The QM of the synchronous average

$$\text{QM}_{\text{SA}}(\boldsymbol{x}) = 10\log\left(\frac{P^{\text{SA}}_{damaged}(\boldsymbol{x})}{P^{\text{SA}}_{healthy}(\boldsymbol{x})}\right), \tag{29}$$

is the last metric that is investigated. The QM of the synchronous average is a function of the ratio of the average power of the damaged portion $P^{\text{SA}}_{damaged}(\boldsymbol{x})$ and the power of the healthy portion $P^{\text{SA}}_{healthy}(\boldsymbol{x})$ of the synchronous average of the signal $\boldsymbol{x}$. A large $\text{QM}_{\text{SA}}(\boldsymbol{x})$ indicates that the synchronous averaged $\boldsymbol{x}$'s average power of the damaged portion is more significant than the average power of the healthy portion. This healthy portion and the damaged portions are calculated with the procedure given in Appendix B. The metric is used for the synchronous averaged vibration signals as well as the synchronously averaged square envelope.

The four metrics are presented in Figure 18 for the damaged measurements, with the kurtosis of the synchronous averaged signals shown. It is evident from the various metrics that the novel

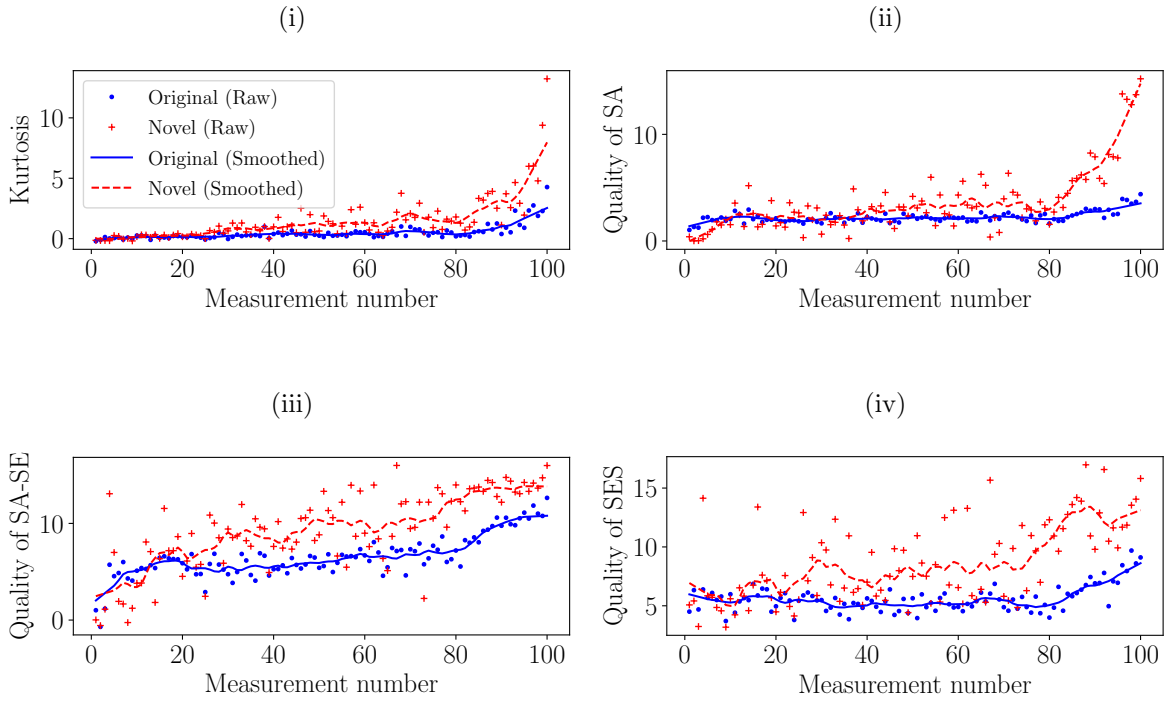

Figure 18: Different metrics of the healthy and the damaged vibration signals are compared for the original and novel signals. The raw metrics, denoted by (*Raw*) in the legend, are calculated by using Equation (27), (28) and (29) on each measurement, where the smoothed estimate is calculated with a moving average with length eight and an overlap of six.

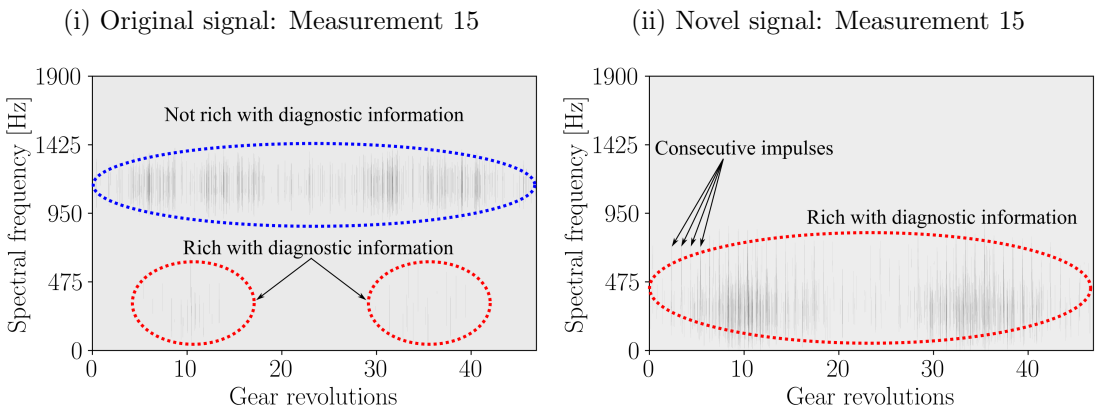

Figure 19: The Angle-Frequency Instantaneous Power Spectrum (AF-IPS) for the vibration signal of a damaged gearbox is presented. Figure 19(i) contains the AF-IPS of the raw vibration signal and Figure 19(ii) contains the AF-IPS for the corresponding novel signal. The two plots are not on the same scales to highlight the dominant components better.

signal is more sensitive to damage when compared to the original signal. However, the quality of the novel signal can vary over time, depending on the noise characteristics of the signal. If the long term data are effectively used i.e. by smoothing the results, it is evident from the results that the novel signal is significantly more sensitive to damage.

4.2.3. Additional analyses

The Instantaneous Power Spectrum (IPS) is also a powerful cyclostationary analysis tool which has been successful for gearbox diagnostics under varying operating conditions [41–43]. The spectrogram estimator of the time-frequency IPS, given by [11]

$$I_{\text{TF-IPS}}[n,m] = \frac{1}{f_s \cdot N_x \cdot \sum_{a=0}^{N_w-1} \upsilon[a]} \left| \sum_{k=0}^{N_w-1} \upsilon[k] \cdot x[k + n \cdot (N_w - N_o)] \cdot e^{-j2\pi km/N_w} \right|^2, \quad (30)$$

is inappropriate for varying speed conditions and therefore the Angle-Frequency IPS (AF-IPS), obtained from order tracking each frequency band of the time-frequency IPS separately [11]

$$I_{\text{AF-IPS}}[a,m] = \text{OT}_{n\to a}\left(I_{\text{TF-IPS}}[n,m]\right) \quad (31)$$

where $\text{OT}_{n\to a}(\cdot)$ indicates that the time index n is converted to an angle index a through order tracking [44, 45]. The AF-IPS is presented in Figure 19 for the original vibration signal of the damaged gearbox and its corresponding novel vibration signal. Two frequency bands, centred approximately at 400Hz and 1100Hz, are highlighted in the IPS of the original signal in Figure

19(i). The non-diagnostic frequency band at 1100Hz dominates the IPS and makes the diagnostic rich frequency band difficult to identify. This is in contrast to the results of the novel signal in Figure 19(ii). The non-diagnostic frequency band at 1100Hz is attenuated, because it was excited in the reference condition and therefore only the diagnostic rich frequency band, which contains the impulses due to the gear damage, is seen in the IPS.

The instantaneous power spectra in Figure 19 provide additional insights into the performance of the original and the novel signals. In the novel signal, the dominant frequency band without diagnostic information is attenuated, while only the frequency band that is rich with diagnostic information is retained. This makes it more sensitive to changes in the condition of the machine. Even though the IPS is a very powerful representation, it can be difficult to interpret and therefore a more intuitive representation is investigated next.

Urbanek et al. [42] illustrated the efficiency of the synchronous averaged IPS to perform bearing diagnostics under varying operating conditions. This reduced the influence of varying operating conditions and non-synchronous components and therefore highlighted the repetitive diagnostic information. Therefore, the marginal synchronous average of the IPS i.e. by marginalising over the N_f spectral frequency bands

$$\bar{i}_{\text{AF-IPS}}[a] = \frac{1}{N_{rot} \cdot N_f} \sum_{m=0}^{N_f-1} \sum_{k=0}^{N_{rot}-1} I_{\text{AF-IPS}}[a + N_s \cdot k, m] \tag{32}$$

is investigated to highlight the localised gear damage and it makes it easier to illustrate the benefits of using the novel signal as opposed to the original signal. The marginal synchronous average of the IPS is presented in Figure 20 for the corresponding results presented in Figure 19(i) and Figure 19(ii). Clearly, the presence of the frequency band that does not contain diagnostic information in Figure 19(i) adversely influences the ability to detect the localised gear damage in Figures 20(i) and 20(iii). In the marginal IPS of the novel signal, presented in Figures 20(ii) and 20(iv), the damage is very prominent and clear, with the non-diagnostic information attenuated.

Hence, it is evident from the results that there are considerable benefits in incorporating historical information in the diagnosis procedure. Hence, it is possible to enhance the ability of existing signal processing techniques to detect damage, characterise damage and trend damage for gear diagnostics under varying operating conditions.

5. Conclusion and recommendations

A methodology is proposed in this paper to extract a novel signal from a vibration signal acquired from a rotating machine. The novel signal is calculated by enhancing the novel infor-

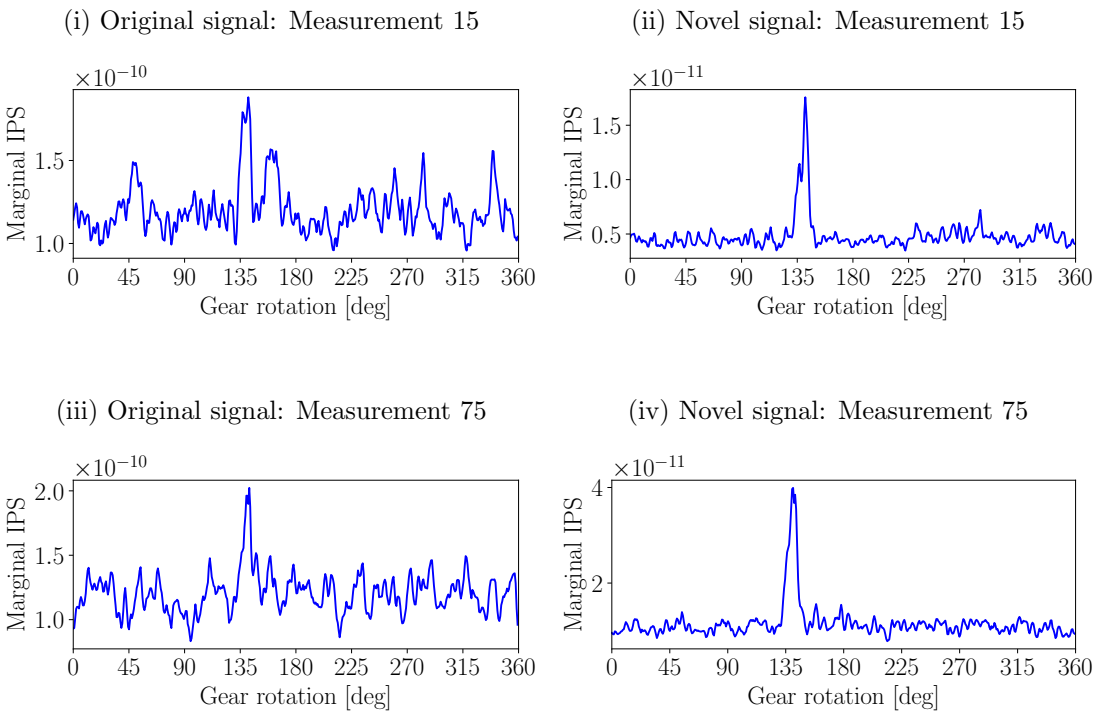

Figure 20: The marginal synchronous averages of the instantaneous power spectra shown in Figure 19 are presented.

mation i.e. the new information that is not present in the available historical reference data, and with the benefit that the novel signal can be processed with standard vibration analysis techniques. It is illustrated on numerical gearbox data and experimental gearbox data that the novel vibration signal is more sensitive to the presence of damage than the original vibration signal. Hence, the methodology can be used as a pre-processing technique to conveniently incorporate historical information into the analysis procedure, without restricting the analysis techniques that could be used.

The methodology is dependent on the availability of historical data in a reference condition, the quality of the features that are used, and the ability to model the features that are used. Hence, future work should focus on making the methodology more robust by optimising each step of the methodology. In summary, these are potential future avenues that could be investigated:

- A faster decomposition of the signal into the feature plane by using an equivalent procedure as the fast kurtogram [17].
- An investigation of using different features e.g. the SES infogram and by simultaneously using a combination of features in the modelling procedure.

- More sophisticated feature modelling procedures need to be investigated to see how much the results can be improved.
- Different novelty detection filters could be investigated where the magnitude of the narrowband signal increases as the degree of novelty in the frequency band increases.
- Investigations should be performed on more datasets to further validate the methodology.

Acknowledgements

The authors gratefully acknowledge the support that was received from the Eskom Power Plant Engineering Institute (EPPEI) in the execution of the research. K.C. Gryllias gratefully acknowledges the Research Fund KU Leuven.

Appendix A. Phenomenological gearbox model

The signal components are presented in Figure A.1 over measurement time. The amplitude modulation due to the rotational speed variation is clearly observed for the signal components. The Signal-to-Noise Ratio (SNR) of the different signal components are presented in Table A.1

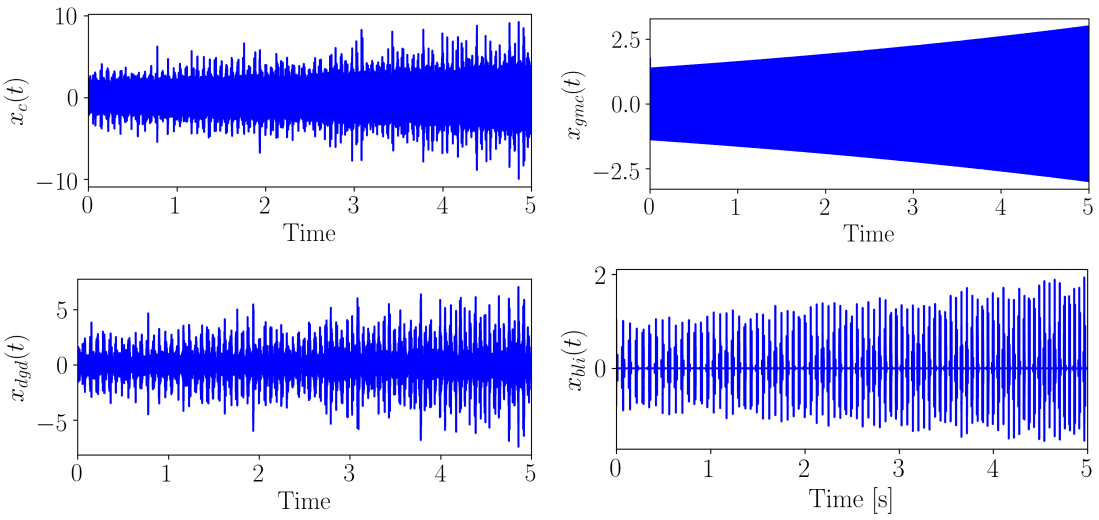

Figure A.1: The casing (x_c), gear mesh (x_{gmc}), distributed gear damage (x_{dgd}) and the inner bearing damage (x_{bli}) signal components are presented for the bearing in the following condition: $FS_{bli} = 1$ and $FS_{blo} = 0$.

for the different bearing conditions.

The natural frequencies and the damping ratios of the single degree-of-freedom impulse response functions used in Equation (17), Equation (18), Equation (19) and Equation (20) are presented in Table A.2.

Table A.1: The Signal-to-Noise Ratio (SNR) in decibels is given of the each signal component in Equation (16). The casing vibration signal's SNR is the average SNR for all considered bearing conditions.

	$x_c(t)$	$x_{gmc}(t)$	$x_{gdd}(t)$	$FS_{bli} \cdot x_{bli}(t)$ $(FS_{bli} = 1)$	$FS_{bli} \cdot x_{bli}(t)$ $(FS_{bli} = 4\ )$	$FS_{blo} \cdot x_{blo}(t)$ $(FS_{blo} = 1)$	$FS_{blo} \cdot x_{blo}(t)$ $(FS_{blo} = 1)$
SNR_{db}	12.893	10.748	8.142	-11.163	1.137	-6.847	5.284

Table A.2: The natural frequency and damping ratio associated with the single degree-of-freedom impulse response function h_i of each component i.

	Natural frequency [Hz]	Damping ratio
Gear mesh component	1000	0.05
Distributed gear damage component	1300	0.05
Inner race bearing component	5500	0.05
Outer race bearing component	7000	0.05

Appendix B. Calculating the SES and SA quality metrics

The calculation of the quality metrics used in Section 4 are presented in Figure B.1. The Quality Metric (QM) of the Squared Envelope Spectrum (SES) is calculated with Equation (28) where the average component of the fault frequency components shown in Figure B.1 is denoted by $\text{SES}_{damaged}$. The SES of the noise floor is calculated by calculating the median of the SES in the frequency range shown in Figure B.1, with the identified fault frequency amplitudes ignored.

The QM of the synchronous average is calculated with Equation 29. The healthy and damaged portions are known beforehand as shown in Figure B.1. Therefore, the power of the healthy and damaged portions shown in Figure B.1 can easily be calculated and is used in Equation (29).

Table A.3: The amplitude and phase of the gear mesh component and the distributed gear damage component. The i can denote the distributed gear damage component gdd in Equation (18) or the gear mesh component gmc in Equation (17).

k	1	2	3
$A_i^{(k)}$	1	2	3
$\varphi_i^{(k)}$	0	0	0

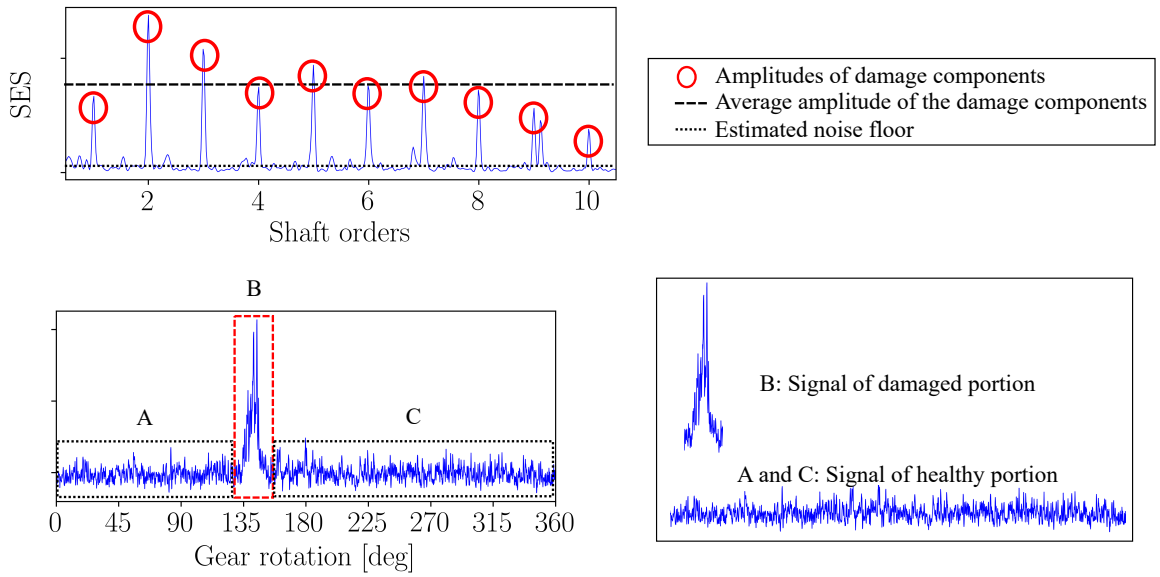

Figure B.1: A supplementary figure to illustrate how the quality of the synchronous average and of the squared envelope spectrum is calculated.

References

[1] A. K. S. Jardine, D. Lin, D. Banjevic, A review on machinery diagnostics and prognostics implementing condition-based maintenance, Mechanical Systems and Signal Processing 20 (7) (2006) 1483–1510.

[2] Y. Lei, J. Lin, Z. He, M. J. Zuo, A review on empirical mode decomposition in fault diagnosis of rotating machinery, Mechanical Systems and Signal Processing 35 (1-2) (2013) 108–126.

[3] J. Antoni, Cyclostationarity by examples, Mechanical Systems and Signal Processing 23 (4) (2009) 987–1036.

[4] Z. K. Peng, F. L. Chu, Application of the wavelet transform in machine condition monitoring and fault diagnostics: A review with bibliography, Mechanical Systems and Signal Processing 18 (2) (2004) 199–221.

[5] R. B. Randall, J. Antoni, Rolling element bearing diagnostics-A tutorial, Mechanical Systems and Signal Processing 25 (2) (2011) 485–520.

[6] J. Antoni, F. Bonnardot, A. Raad, M. El Badaoui, Cyclostationary modelling of rotating machine vibration signals, Mechanical Systems and Signal Processing 18 (6) (2004) 1285–1314.

[7] D. Abboud, S. Baudin, J. Antoni, D. Rémond, M. Eltabach, O. Sauvage, The spectral analysis of cyclo-non-stationary signals, Mechanical Systems and Signal Processing 75 (2016) 280–300.

[8] J. Antoni, Cyclic spectral analysis of rolling-element bearing signals: Facts and fictions, Journal of Sound and Vibration 304 (2007) 497–529.

[9] J. Antoni, Cyclic spectral analysis in practice, Mechanical Systems and Signal Processing 21 (2007) 597–630.

[10] D. Abboud, J. Antoni, M. Eltabach, S. Sieg-zieba, Angle\time cyclostationarity for the analysis of rolling element bearing vibrations, Measurement 75 (2015) 29–39.

[11] D. Abboud, J. Antoni, Order-frequency analysis of machine signals, Mechanical Systems and Signal Processing 87 (October 2016) (2017) 229–258.

[12] D. Abboud, J. Antoni, S. Sieg-Zieba, M. Eltabach, Envelope analysis of rotating machine vibrations in variable speed conditions: A comprehensive treatment, Mechanical Systems and Signal Processing 84 (2017) 200–226.

[13] P. Borghesani, R. Ricci, S. Chatterton, P. Pennacchi, A new procedure for using envelope analysis for rolling element bearing diagnostics in variable operating conditions, Mechanical Systems and Signal Processing 38 (1) (2013) 23–35.

[14] P. Borghesani, P. Pennacchi, R. B. Randall, N. Sawalhi, R. Ricci, Application of cepstrum pre-whitening for the diagnosis of bearing faults under variable speed conditions, Mechanical Systems and Signal Processing 36 (2) (2013) 370–384.

[15] J. Antoni, The spectral kurtosis: A useful tool for characterising non-stationary signals, Mechanical Systems and Signal Processing 20 (2) (2006) 282–307.

[16] J. Antoni, R. B. Randall, The spectral kurtosis: Application to the vibratory surveillance and diagnostics of rotating machines, Mechanical Systems and Signal Processing 20 (2) (2006) 308–331.

[17] J. Antoni, Fast computation of the kurtogram for the detection of transient faults, Mechanical Systems and Signal Processing 21 (2007) 108–124.

[18] T. Barszcz, R. B. Randall, Application of spectral kurtosis for detection of a tooth crack in the planetary gear of a wind turbine, Mechanical Systems and Signal Processing 23 (4) (2009) 1352–1365.

[19] F. Combet, L. Gelman, Optimal filtering of gear signals for early damage detection based on the spectral kurtosis, Mechanical Systems and Signal Processing 23 (3) (2009) 652–668.

[20] J. Antoni, The infogram: Entropic evidence of the signature of repetitive transients, Mechanical Systems and Signal Processing 74 (2016) 73–94.

[21] T. Barszcz, A. Jabłoński, A novel method for the optimal band selection for vibration signal demodulation and comparison with the Kurtogram, Mechanical Systems and Signal Processing 25 (1) (2011) 431–451.

[22] Y. Lei, J. Lin, Z. He, Y. Zi, Application of an improved kurtogram method for fault diagnosis of rolling element bearings, Mechanical Systems and Signal Processing 25 (5) (2011) 1738–1749.

[23] D. Wang, P. W. Tse, K. L. Tsui, An enhanced Kurtogram method for fault diagnosis of rolling element bearings, Mechanical Systems and Signal Processing 35 (1-2) (2013) 176–199.

[24] W. A. Smith, Z. Fan, Z. Peng, H. Li, R. B. Randall, Optimised Spectral Kurtosis for bearing diagnostics under electromagnetic interference, Mechanical Systems and Signal Processing 75 (2015) 371–394.

[25] P. W. Tse, D. Wang, The design of a new sparsogram for fast bearing fault diagnosis: Part 1 of the two related manuscripts that have a joint title as "two automatic vibration-based fault diagnostic methods using the novel sparsity measurement - Parts 1 and 2", Mechanical Systems and Signal Processing 40 (2) (2013) 499–519.

[26] J. Obuchowski, A. Wylomanska, R. Zimroz, Selection of informative frequency band in local damage detection in rotating machinery, Mechanical Systems and Signal Processing 48 (1-2) (2014) 138–152.

[27] X. Xu, M. Zhao, J. Lin, Y. Lei, Envelope harmonic-to-noise ratio for periodic impulses detection and its application to bearing diagnosis, Measurement 91 (2016) 385–397.

[28] A. Moshrefzadeh, A. Fasana, The autogram: An effective approach for selecting the optimal demodulation band in rolling element bearings diagnosis, Mechanical Systems and Signal Processing 105 (2018) 294–318.

[29] D. Wang, An extension of the infograms to novel Bayesian inference for bearing fault feature identification, Mechanical Systems and Signal Processing 80 (2016) 19–30.

[30] X. Xu, Z. Qiao, Y. Lei, Repetitive transient extraction for machinery fault diagnosis using multiscale fractional order entropy infogram, Mechanical Systems and Signal Processing 103 (2018) 312–326.

[31] R. B. Randall, Detection and diagnosis of incipient bearing failure in helicopter gearboxes, Engineering Failure Analysis 11 (2) (2004) 177–190.

[32] D. Fernández-Francos, D. Martínez-Rego, O. Fontenla-Romero, A. Alonso-Betanzos, Automatic bearing fault diagnosis based on one-class ν-SVM, Computers & Industrial Engineering 64 (1) (2013) 357–365.

[33] R. Klein, E. Masad, E. Rudyk, I. Winkler, Bearing diagnostics using image processing methods, Mechanical Systems and Signal Processing 45 (1) (2014) 105–113.

[34] E. Jones, T. Oliphant, P. Peterson, et al., SciPy: Open source scientific tools for Python, [Online; accessed 2018-09-05] (2001–).
URL http://www.scipy.org/

[35] P. D. McFadden, J. D. Smith, Vibration monitoring of rolling element bearings by the high-frequency resonance technique - A review, Tribology International 17 (1) (1984) 3–10.

[36] D. Abboud, J. Antoni, S. Sieg-Zieba, M. Eltabach, Deterministic-random separation in nonstationary regime, Journal of Sound and Vibration 362 (2016) 305–326.

[37] J. Antoni, G. Xin, N. Hamzaoui, Fast computation of the spectral correlation, Mechanical Systems and Signal Processing 92 (2017) 248–277.

[38] C. J. Stander, P. S. Heyns, W. Schoombie, Using vibration monitoring for local fault detection on gears operating under fluctuating load conditions, Mechanical Systems and Signal Processing 16 (6) (2002) 1005–1024.

[39] C. J. Stander, P. S. Heyns, Instantaneous angular speed monitoring of gearboxes under non-cyclic stationary load conditions, Mechanical Systems and Signal Processing 19 (4) (2005) 817–835.

[40] S. Schmidt, P. S. Heyns, J. P. de Villiers, A novelty detection diagnostic methodology for gearboxes operating under fluctuating operating conditions using probabilistic techniques, Mechanical Systems and Signal Processing 100 (2018) 152–166.

[41] N. Baydar, A. Ball, Detection of gear deterioration under varying load conditions by using the instantaneous power spectrum, Mechanical Systems and Signal Processing 14 (6) (2000) 907–921.

[42] J. Urbanek, T. Barszcz, R. Zimroz, J. Antoni, Application of averaged instantaneous power spectrum for diagnostics of machinery operating under non-stationary operational conditions, Measurement 45 (7) (2012) 1782–1791.

[43] J. Urbanek, T. Barszcz, J. Antoni, Time-frequency approach to extraction of selected second-order cyclostationary vibration components for varying operational conditions, Measurement: Journal of the International Measurement Confederation 46 (4) (2013) 1454–1463.

[44] K. Fyfe, E. Munck, Analysis of computed order tracking, Mechanical Systems and Signal Processing 11 (2) (1997) 187–205.

[45] Q. Leclère, H. André, J. Antoni, A multi-order probabilistic approach for Instantaneous Angular Speed tracking debriefing of the CMMNO'14 diagnosis contest, Mechanical Systems and Signal Processing 81 (2016) 375–386.